

GL-TR-90-0084

EFFECTS OF ENERGY, MOMENTUM AND PARTICLE
TRANSPORT IN THE NEAR-EARTH SOLAR
TERRESTRIAL SYSTEM

P. B. Anderson
E. M. Basinska-Lewin
M. E. Greenspan
J. H. James
D. R. Weimer

Regis College Research Center
235 Wellesley Street
Weston, MA 02193

AD-A224 393

01 June 1990

DTIC
ELECTE
JUL 30 1990
S D D^{CS}

Final Report
02 December 1986 - 01 May 1990

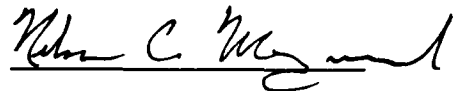
Approved for public release; distribution unlimited

GEOPHYSICS LABORATORY
AIR FORCE SYSTEMS COMMAND
UNITED STATES AIR FORCE
HANSCOM AIR FORCE BASE, MASSACHUSETTS 01731-5000

"This Technical report has been reviewed and is approved for publication"



FREDERICK J. RICH
Contract Manager



NELSON C. MAYNARD
Branch Chief

FOR THE COMMANDER



RITA C. SAGALYN
Division Director

This report has been reviewed by the ESD Public Affairs Office (PA) and is releasable to the National Technical Information Service (NTIS).

Qualified requestors may obtain additional copies from the Defense Technical Information Center. All others should apply to the National Technical Information Service.

If your address has changed, or if you wish to be removed from the mailing list, or if the addressee is no longer employed by your organization, please notify GL/IMA, Hanscom AFB, MA 01731. This will assist us in maintaining a current mailing list.

Do not return copies of this report unless contractual obligations or notices on a specific document requires that it be returned.

REPORT DOCUMENTATION PAGE

Form Approved
OMB No. 0704-0188

Public reporting burden for this collection of information is estimated to average 1 hour per response, including the time for reviewing instructions, searching existing data sources, gathering and maintaining the data needed, and completing and reviewing the collection of information. Send comments regarding this burden estimate or any other aspect of the collection of information, including suggestions for reducing this burden, to Washington Headquarters Services, Directorate for Information Operations and Reports, 1215 Jefferson Davis Highway, Suite 1204, Arlington, VA 22202-4302, and to the Office of Management and Budget, Paperwork Reduction Project (0704-0188), Washington, DC 20503

1. AGENCY USE ONLY (Leave blank)	2. REPORT DATE 01 June 1990	3. REPORT TYPE AND DATES COVERED Final Report (2 Dec 1986 - 1 May 1990)	
4. TITLE AND SUBTITLE Effects of Energy, Momentum and Particle Transport in the Near-Earth Solar Terrestrial System		5. FUNDING NUMBERS PE 63220C PR S321 TA 10 WU AA Contract F19628-86-K-00	
6. AUTHOR(S) P. B. Anderson E. M. Basinska-Lewin M. E. Greenspan J. H. James D. R. Weimer		8. PERFORMING ORGANIZATION REPORT NUMBER	
7. PERFORMING ORGANIZATION NAME(S) AND ADDRESS(ES) Regis College Research Center 235 Wellesley Street Weston, MA 02193		10. SPONSORING / MONITORING AGENCY REPORT NUMBER GL-TR-90-0084	
9. SPONSORING / MONITORING AGENCY NAME(S) AND ADDRESS(ES) Geophysics Laboratory Hanscom AFB Massachusetts 01731-5000 Contract Manager: Frederick Rich/PHG		11. SUPPLEMENTARY NOTES	
12a. DISTRIBUTION / AVAILABILITY STATEMENT Approved for public release; distribution unlimited.		12b. DISTRIBUTION CODE	
13. ABSTRACT (Maximum 200 words) A summary is given of the work completed under contract F19628-86-K-0045; this work has included the scientific studies of high-latitude plasma irregularities and the physics of the aurora, engineering of space environmental sensors, and data processing services. Scientific studies were conducted in the areas of energy dissipation, magnetosphere-ionosphere interactions and ionospheric plasma. Design work has been done on a series of plasma instruments for the Defense Meteorological Satellite Program (DMSP), the Combined Release and Radiation Effects Studies (CRRES), the Photovoltaic Array Space Power (PASP), the Interactions Measurements Payload for Shuttle (IMPS) and the NASA POLAR satellite program. Computer programs have been written to process RPA and Drift Meter data from the F8 and F9 DMSP satellites.			
14. SUBJECT TERMS Ionosphere, magnetosphere, auroral electrojet, auroral currents, electric fields, magnetic fields, plasma irregularities, cusp, DMSP, DE-1, DE-2, ISEE-1, ISEE-2, S3-2, SSIES, SSIES-2, CRRES.		15. NUMBER OF PAGES 84	16. PRICE CODE
17. SECURITY CLASSIFICATION OF REPORT Unclassified	18. SECURITY CLASSIFICATION OF THIS PAGE Unclassified	19. SECURITY CLASSIFICATION OF ABSTRACT Unclassified	20. LIMITATION OF ABSTRACT SAR

Table of Contents

1. INTRODUCTION	1
2. ENERGY DISSIPATION	3
2.1 Statistical Model of Joule Heating From DMSP Data	3
2.2 Electric Potentials and Auroral Electrojet Indices	4
3. MAGNETOSPHERE-IONOSPHERE INTERACTIONS	11
3.1 Auroral Current Oscillations	11
3.2 Magnetic Field-Line Conductivity	12
3.3 Low-Altitude Signatures of the Flux Transfer Events	13
3.4 Field and Particle Characteristics in DE-2 Crossings of the Low Cusp/Cleft Regions	
17	
3.4.1 Intense Electric Fields at the Equatorward Boundary of the Dayside Cusp ..	17
3.5 An Equation for Field-Aligned Current	21
3.6 Collaborative Studies of Ionospheric Signatures of Magnetospheric Boundary Regions	
23	
4. IONOSPHERIC PLASMA STUDIES	38
4.1 Midlatitude and Equatorial Ion Morphology at Solar Minimum	38
4.2 Density Depletions Observed at 840 km During the Great Magnetic Storm of March	
1989	39
5. DESIGN OF SPACE ENVIRONMENTAL SENSORS	45
5.1 Introduction	45

5.2 DMSP: SSIES & SSIES-2	45
5.2.1 SSIES & SSIES-2 Overview	45
5.2.2.1 SSIES Activity	46
5.2.2.2 SSIES-2 Activity	47
5.3 CRRES	48
5.3.1 CRRES Overview	48
5.3.1.1 AFGL-701-13-1 Overview	49
5.3.1.2 AFGL-701-13-2 Overview	49
5.3.1.3 AFGL-701-14 Overview	49
5.3.1.4 AFGL-701-15 Overview	50
5.3.2.1 CRRES-225 Activity	50
5.3.2.2 AFGL-701-13-1 Activity	51
5.3.2.3 AFGL-701-14 Activity	51
5.3.2.4 AFGL-701-15 Activity	52
5.4 PASP	52
5.4.1 PASP Overview	52
5.4.2 PASP Activity	53
5.5 IMPS	53
5.5.1 IMPS Overview	53
5.5.2 IMPS Activity	54

5.6 POLAR	54
5.6.1 POLAR Overview	54
5.6.2 POLAR Activity	55
6. DATA PROCESSING AND ANALYSIS	66
6.1 SSIES Data Processing	66
6.2 RPA Sweep Analysis Program	67
6.3 Removal of Corotation from SSIES Drift Data	70
6.4 Digitizing Models of Plasma Convection	71
7. PUBLICATIONS	77



Accession For	
NTIS CRA&I	<input checked="" type="checkbox"/>
DTIC TAB	<input type="checkbox"/>
Unannounced	<input type="checkbox"/>
Justification	
By	
Distribution/	
Availability Codes	
Dist	Avail and/or Special
A-1	

1. INTRODUCTION

This report covers the work accomplished by Regis College under contract F19628-86-K-0045 with the Geophysics Laboratory (GL). Scientific studies completed under this contract relate to energy dissipation, magnetosphere-ionosphere interactions ionospheric plasma. Computer programs were written in support of the scientific studies for processing space environmental data. Other activities included providing design services for space environmental sensors. A summary of the accomplishments follows:

- a. Participated in a study of Joule heat energy flow into the high latitude ionosphere. As a result, a reasonable estimate was made of the height-integrated Joule heating in the E-region ionosphere.
- b. Conducted an investigation to learn if the polar cap potential drop can be derived from the auroral electrojet index.
- c. Completed studies of electric and magnetic fields measured near magnetic conjunctions of two Dynamics Explorer satellites. This study focused on when a spatial oscillation in the magnetic field-aligned current is present.
- d. Developed methodology for use by investigators to identify the ionosphere signature of Flux Transfer Events (FTE) based on expected, simultaneous measurements of electric fields (plasma drifts), magnetic fields (field-aligned currents) and precipitating particle fluxes.
- e. Studied the morphology of the thermal plasma ions measured by a DMSP satellite during the solar minimum period and density depletions observed by DMSP satellites during the great magnetic storm of March 1989.
- f. Provided engineering resources for the development of several space environmental

sensors. This work has included instrument design, evaluation, calibration and spacecraft integration.

g. Performed data processing to support the scientific analysis of the space environmental data from DMSP satellites. This activity required the development of a sophisticated data reduction program for merging the drift meter and RPA measurements of ion drift velocity to get the complete drift velocity vector, subtracts corotation from the ion drift, and rotates the model magnetic field into the same coordinates as the ion drift.

The remainder of this report consists of brief descriptions of the work done under this contract. A list of papers and publications generated as a result of work done in whole or part of this contract is contained in Chapter 7. In cases where the results of work done on this contract have been published, only brief summaries of the result are contained in this Final Report; the referenced publications should be consulted for specific details about the research. For the case where the research results have not been published, more detailed accounts of the work are given in this report.

2. ENERGY DISSIPATION

2.1 Statistical Model of Joule Heating From DMSP Data

Energy transferred from the magnetosphere to the thermosphere via the ionosphere is important in determining thermospheric dynamics and structure. In turn, the behavior of the thermosphere affects the orbits and lifetimes of low-altitude satellites. Much of the energy transfer from magnetosphere to thermosphere occurs at high latitudes through Joule heating. Thus, determining the energy transferred to the thermosphere through Joule heating is an important goal.

Regis College personnel participated in a preliminary study of Joule heat energy flow into the high latitude ionosphere. This study is described in detail in Rich et al.¹. Particle and magnetic field data from the DMSP F7 satellite were combined to estimate the Joule heat input once each second at the foot of the field line intercepting the satellite track. The ionospheric conductivity was calculated from the precipitating electron spectra, the 10.7 cm radio flux, and the solar zenith, using the formulas of Robinson et al.² and Robinson and Vondrak³. Ionospheric Pederson currents were calculated from the magnetometer data, using the assumption that field-aligned currents flow in infinite sheets and close locally beneath the satellite.

Early results showed that this method gave a reasonable estimate of height-integrated Joule heating in the E-region ionosphere. As expected, Joule heating was greatest in the auroral oval. Indications of Joule heating were also seen in the dayside cup/cleft region.

¹ Rich, F. J., M. S. Gussenhoven, and M. E. Greenspan, Using simultaneous particle and field observations on a low altitude satellite to estimate Joule heat energy flow into the high latitude ionosphere, *Ann. Geophys.* 5A, 527-534, 1987.

² Robinson, R. M., R. R. Vondrak, K. Miller, T. Dabs, and D. Hardy, On calculating ionospheric conductances from the flux and energy of precipitating electrons, *J. Geophys. Res.* 92, 2565-2569, 1987.

³ Robinson, R. M. and R. R. Vondrak, Measurements of E region ionization and conductivity produced by solar illumination at high latitudes, *J. Geophys. Res.* 89, 3951-3956, 1984.

This method may be used in the future to develop a statistical map of Joule heating in the high-latitude ionosphere.

2.2 Electric Potentials and Auroral Electrojet Indices

It would be useful (to those who need to calculate and predict the orbits of low-altitude satellites) to be able to continuously monitor the energy dissipation in the high-latitude ionosphere. If the electric field and ionospheric conductivity over the entire polar cap and auroral zones could be measured on a continuous basis, then a "real-time" calculation of the global Joule heating would be possible. Unfortunately, the electric fields and conductivities which can be measured by satellites have limited spatial and temporal coverage, so it has been necessary to resort to statistical analysis in order to derive "average" patterns, such as the conductivity model by Hardy et al.⁴ . Patterns for the electric field have been developed by Heppner and Maynard⁵ and modified by Rich and Maynard⁶ .

Electric field models can be characterized by the total voltage across the polar cap. Eventually it may be possible to develop an electric field model which can be scaled according to this polar cap potential drop. Then if the potential drop could be measured in "real-time", the global electric field would also be known (within the accuracy of the model) in real-time.

Electrical currents in the high-latitude ionosphere are monitored continuously by a ground-based network of magnetometers. The Auroral Electrojet (AE) index is obtained from these magnetic field measurements. An investigation has been conducted by Regis College to learn if the polar cap potential drop can be derived from the AE index. Full details

⁴ Hardy, D. A., M. S. Gussenhoven, R. Raistrick, and W. J. McNeil, Statistical and functional representations of the patterns of auroral energy flux, number flux, and conductivity, *J. Geophys. Res.*, **92**, 12275, 1987.

⁵ Heppner, J. P., and N. C. Maynard, Empirical high-latitude electric field models, *J. Geophys. Res.*, **92**, 4467, 1987.

⁶ Rich, F. J., and N. C. Maynard, Consequences of using simple analytical functions and the high-latitude convection electric field, *J. Geophys. Res.*, **94**, 3687, 1989.

of this investigation are contained in Publication 8. To summarize, 527 measurements of the polar cap potential obtained with the DE-2 satellite were compared with simultaneous AE indices. Since the relationship will depend on the ionospheric conductivity (which depends on sunlight), the data were grouped according to the season in the northern hemisphere. Figures 2-1 and 2-2 show the results for the summer and winter seasons. The upper and lower solid lines in these figures show the bounds of 80% of the data points. The middle lines were obtained by fitting the data to an equation in which AE is proportional to the potential, but there is a change in the slope at a certain fixed potential. The equation for the fit to the winter data in Figure 2-1 is

$$AE = 2.17\Phi \quad \Phi < 57.38 \text{ kV} \quad (1a)$$

$$AE = 124.5 + 7.25(\Phi - 57.38) \quad \Phi \geq 57.38 \text{ kV} \quad (1b)$$

where AE has units of nanoTesla and Φ is the polar cap potential in kilovolts. The least-error fit for the summer data is given by

$$AE = 3.63\Phi \quad \Phi < 32.86 \text{ kV} \quad (2a)$$

$$AE = 119.3 + 7.47(\Phi - 32.86) \quad \Phi \geq 32.86 \text{ kV} \quad (2b)$$

These equations can be inverted and interpolated between seasons to find the most probable value of the polar cap potential for a given AE index. In Publication 8 the electric potentials across the dawn and dusk auroral zones are also compared with the AL and AU indices.

This research has also helped to shed some light on the physics of magnetospheric substorms. Figures 2-3 and 2-4 show data which have been grouped according to substorm phase in the cases where a clear growth, expansion, or recovery phase could be identified in the plots of the AE index as a function of time. These data indicate that substorm

expansion may occur only when the polar cap potential exceeds approximately 60 kV. This lends some credibility to (but does not necessarily prove) a recent theoretical model for magnetosphere-ionosphere coupling and the substorm process which has been proposed by Kan et al.⁷ .

⁷ Kan, J. R., L. Zhu, and S.-I. Akasofu, A theory of substorms onset and subsidence, *J. Geophys. Res.*, 93, 5624, 1988.

6 NOV 81 - 4 JAN 82

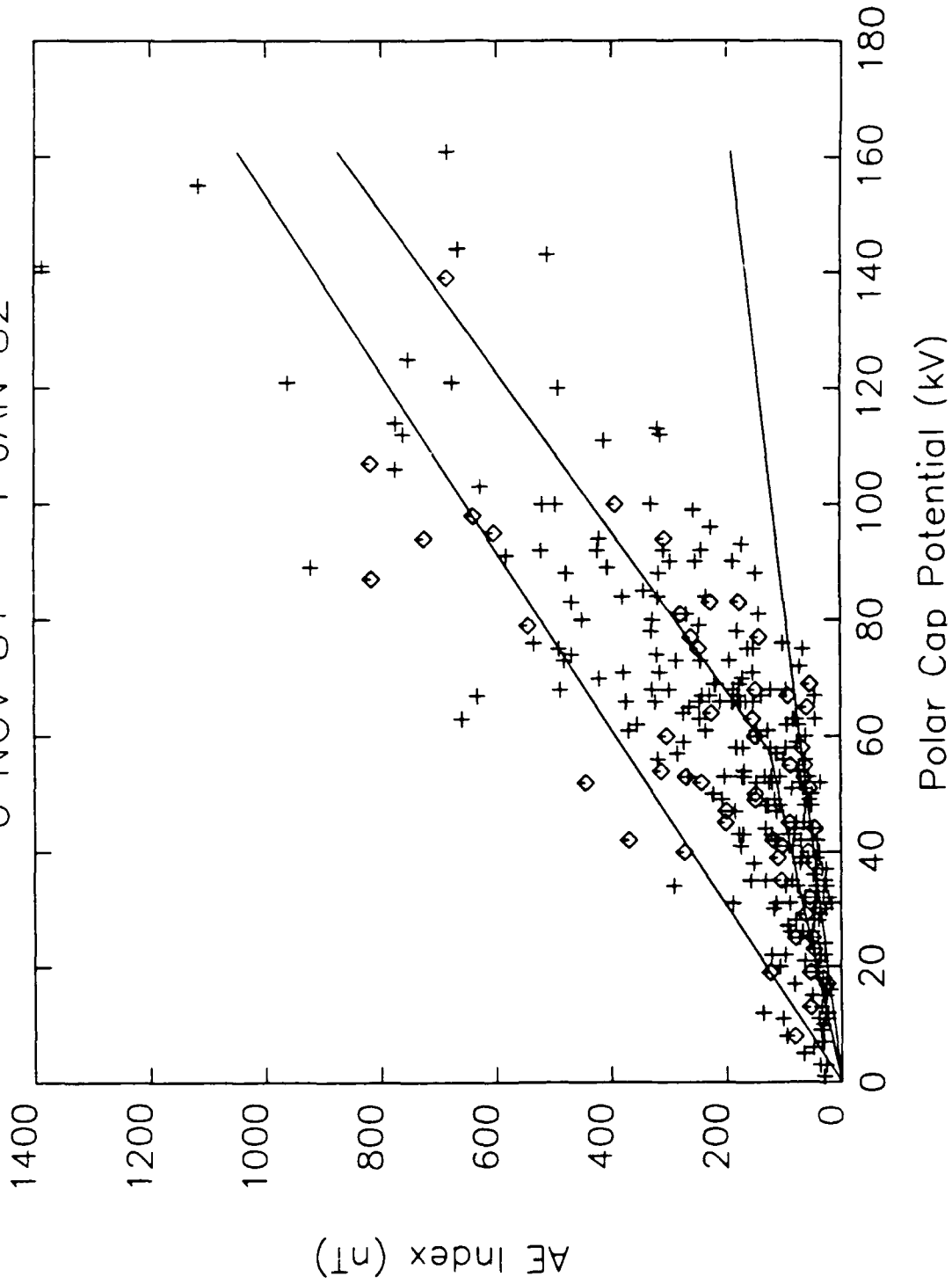


Figure 2-1 Scatter plot of the AE index vs. polar cap potential during winter in the northern hemisphere. The cross marks indicate where the DE-2 satellite measured the potential over the northern hemisphere, and the diamonds indicate measurements over the southern hemisphere polar cap.

1 MAY 82 - 29 JUNE 82

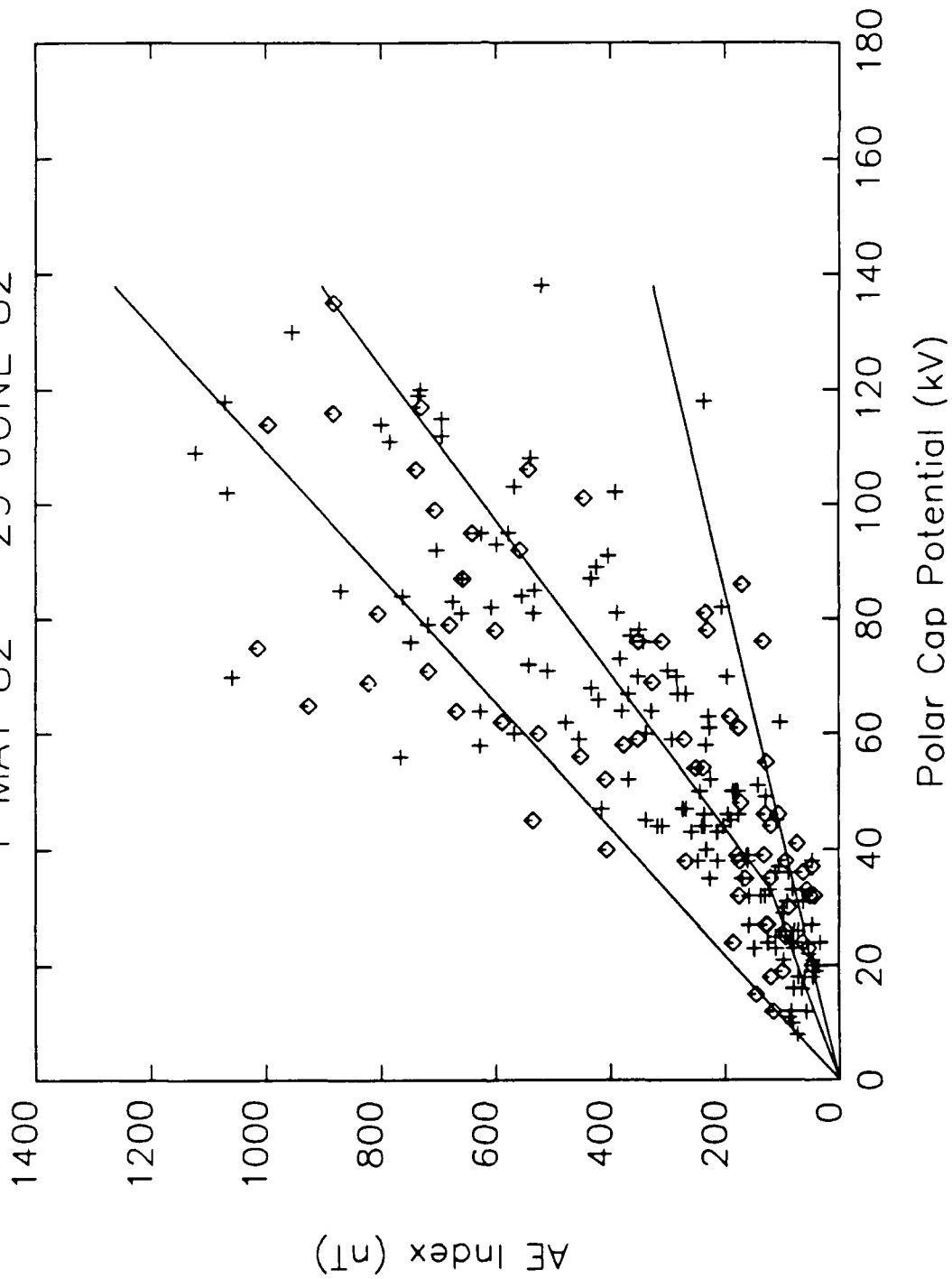


Figure 2-2 Scatter plot of the AE index vs. polar cap potential during summer in the northern hemisphere. The cross marks indicate where the DE-2 satellite measured the potential over the northern hemisphere, and the diamonds indicate measurements over the southern hemisphere polar cap.

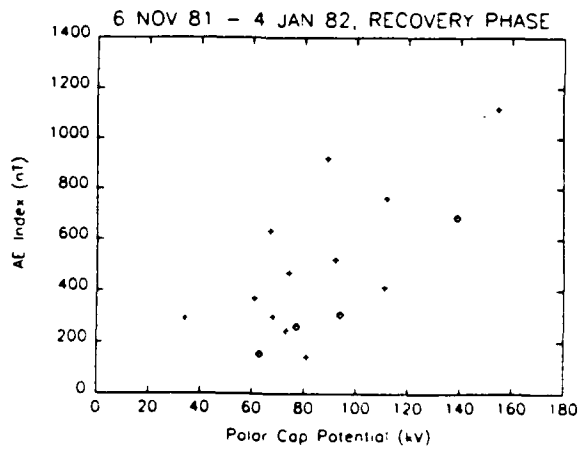
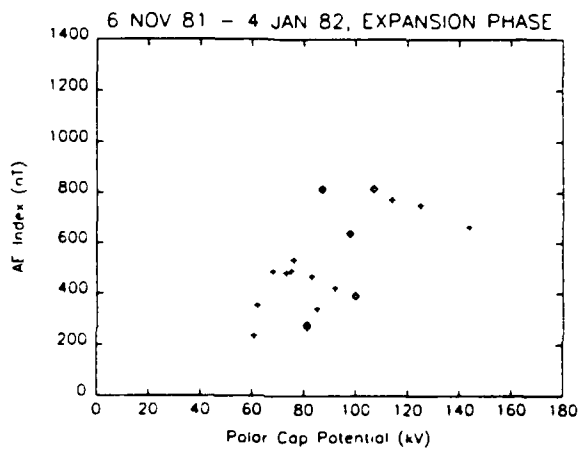
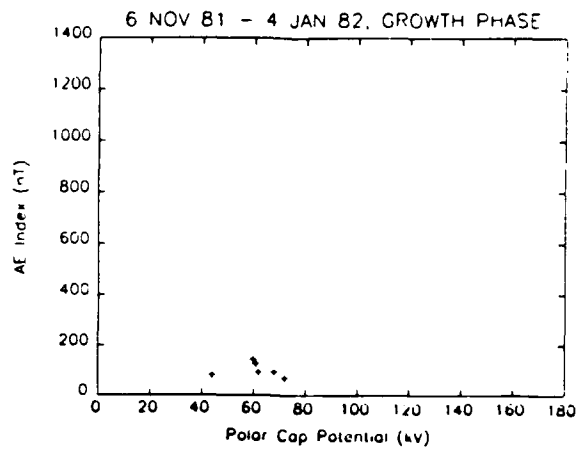


Figure 2-3 AE index vs. polar cap potential for the northern hemisphere winter period, for the cases in which an unambiguous substorm growth, expansion, or recovery phase could be identified.

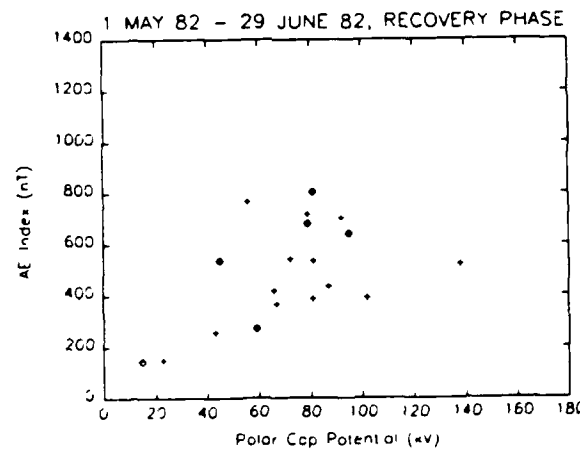
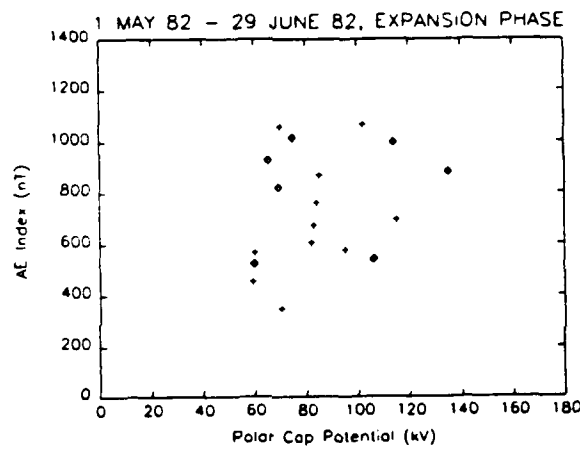
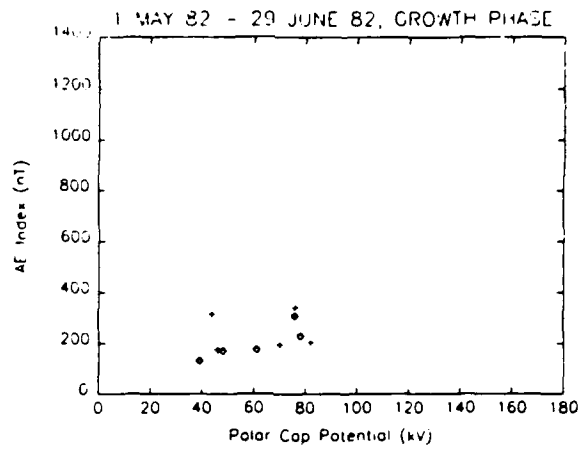


Figure 2-4 AE index vs. polar cap potential for the northern hemisphere summer period, for the cases in which an unambiguous substorm growth, expansion, or recovery phase could be identified.

3. MAGNETOSPHERE-IONOSPHERE INTERACTIONS

3.1 Auroral Current Oscillations

Studies of electric and magnetic fields measured near magnetic conjunctions of the two Dynamics Explorer satellites had turned up an interesting case where a spatial oscillation in the magnetic field-aligned current is present. Figure 3-1 shows the electric field data from DE-1 and DE-2, in which a similar oscillatory form was detected by the two satellites at the same invariant latitude, but separated in time by 20 minutes (hence the identification as a spatial rather than temporal variation). Similar oscillations were present in the magnetic fields, indicating that the field-aligned current consisted of alternating bands of up and downward current.

No explanation for this phenomena had been known, so the physics of the magnetosphere-ionosphere coupling process was studied in order to find out how it was possible for such oscillations to exist. A theory which could explain the oscillations was developed. In this model the oscillation is formed as a result of feedback between a current generator at the magnetospheric equator and the load in the ionosphere. The wavelength of the oscillations depends on the ionospheric height-integrated Pedersen conductivity, the conductivity of the generator, and the parallel conductivity of the magnetic field lines which connect the two regions. The oscillations can occur only if the Pedersen conductivity is greater than the generator conductivity. Figure 3-2 shows the electric fields in this model, in which the electric fields across a 800 km range are nearly a mirror-image of the 800 km span of data in Figure 3-1 between 65 and 73 degrees invariant latitude. The Pedersen and field-line conductivities which were used to derive Figure 3-2 were matched with the observed conditions, and the generator conductivity was determined from the wavelength of

the oscillation. This estimated generator conductivity was found to be within the range of what could be expected, on the basis of magnetohydrodynamic theory. Full details of this work are found in Publication 3. This research has helped to shed light on the physics of M-I coupling.

3.2 Magnetic Field-Line Conductivity

It previously had been shown by Weimer et al.⁸ that the "parallel conductivity" of auroral magnetic field lines could be determined by a nearly-simultaneous measurement of electric fields at two different altitudes. The parallel conductivity should be infinite according to the basic principals of plasma physics; the evidence for a finite conductivity has important implications for auroral physics. A field-aligned electric field is responsible for the acceleration of auroral electrons and plays a key role in the M-I coupling process.

The technique for measuring the parallel conductivity has been improved and refined as a part of the Regis College contract research. The details are given in Publication 4, which is a review paper of electric field measurements by two satellites at conjunctions. To summarize the results, the parallel conductivity is determined by an analysis of the spectrums of the perpendicular electric fields which are measured at different altitudes, above and below the parallel potential drop. The spectrums are derived by a Fourier transform. Originally the spectrums had been smoothed by a sliding average, and then the ratio of the spectrums was fit to a characteristic equation. The fit to the non-linear equation had been done by eye; the improved method does not require the smoothing. Instead, a computer program is used to find the best fit to the equation by a trial-and-error technique, usually referred to as the "simplex method", using the ratio of the unsmoothed spectrums. It also has been shown

⁸ Weimer, D. R., C. K. Goertz, D. A. Gurnett, N. C. Maynard, and J. L. Burch, Auroral zone electric fields from DE 1 and 2 and magnetic conjunctions, *J. Geophys. Res.*, 90, 7479, 1985

that the parallel conductivity can be measured as reliably with only electric and magnetic field measurements on the one high-altitude satellite, instead of requiring a second electric field measurement on a different satellite. An example is in Figure 3-3, which shows the best fit of the characteristic equation to the ratios E_2/E_1 and B_1/E_1 , where the subscripts indicate on which DE satellite the electric (E) or magnetic (B) fields were measured. From the equations

$$\frac{B_1}{E_1} = \frac{\mu_0 \Sigma_p}{1 + (k/k_0)^2} \quad (3)$$

$$k_0^2 = G/\Sigma_p \quad (4)$$

and the fit shown in the right side of Figure 3-3, it is determined that the ionospheric Pedersen conductivity, Σ_p , is 6.46 mho and the parallel, field-line conductivity, G , is 1.1×10^{-8} mho-m⁻².

3.3 Low-Altitude Signatures of the Flux Transfer Events

Flux transfer events (FTEs), discovered by Russell and Elphic (1978)⁹ on the dayside magnetopause in the ISEE 1 and ISEE 2 magnetic field measurements, are believed to be manifestations of intermittent magnetic merging processes. They have been observed near the subsolar portion of the magnetopause for the southward IMF, leaving behind a pair of reconnected flux tubes, one connected to the northern polar cusp, the other to the southern cusp. Typical flux transfer events found in the ISEE survey (Rijnbeek et al., 1984¹⁰; Berchem and Russell, 1984¹¹) have diameters of 1 - 2 R_E near the magnetopause. Magnetic field signatures suggest that FTEs carry field-aligned currents of the order of 1×10^5 A. Their occurrence frequency is estimated to be one every 5 to 10 minutes. The associated magnetic

⁹ Russell and Elphic, Initial ISEE Magnetometer Results, *Space Sci. Rev.*, 22, 681, 1978

¹⁰ Rijnbeek, R.P., S.W.H. Cowley, D.J. Southwood, and C.T. Russell, A Survey of Dayside Flux Transfer Events Observed by ISEE 1 and 2 Magnetometers, *J. Geophys. Res.*, 89, 786, 1984

¹¹ Berchem, J., and C.T. Russell, Flux Transfer Events on the Magnetopause: Spatial Distribution and Controlling Factors, *J.*

flux transfer of about 2×10^6 to 3×10^7 Wb (Cowley, 1982¹²) may represent an important contribution to the polar cap potential.

Since the phenomena occurring in the outer magnetosphere electrically couple to the ionosphere, one expects newly reconnected flux tubes to leave footprints at the ionospheric heights. Disturbances at the magnetopause are transmitted along the field lines by Alfvén waves. If the lifetime of the FTE exceeds Alfvén bounce time ($t_A = 1-2$ min), quasi-static field-aligned current system should develop. The field-aligned current closure through the conducting ionosphere determines the low-altitude characteristics of FTEs. Based on this assumption, McHenry and Clauer (1987)¹³ calculated magnetic field signatures expected during a passage of the ionospheric foot of the FTE over a ground magnetometer station. There is some observational evidence that vestiges of FTEs and other localized magnetopause phenomena (impulsive solar wind disturbances and surface waves) have been detected with variety of ionospheric and ground techniques, but there were no reports of direct observations of FTEs on polar orbiting satellites.

The objective of Publication 6 was to develop criteria useful for identifying the passage of polar orbiting satellites above the ionospheric footprints of FTEs. We assumed that the satellite fly in the altitude range 300 - 1500 km, that is, well above the E layer currents and well below magnetospheric generators and field-aligned potential drops. In this altitude regime, electric and magnetic field perturbations are perpendicular to the main geomagnetic field. Thus the analytical problem reduces to solving two-dimensional Poisson's equations for the scalar and vector potentials defining the electric and magnetic perturbation fields.

Geophys. Res., 89, 6689, 1984

¹² Cowley, S.W.H., The Causes of the Convection in the Earth's Magnetosphere - A Review of Developments during the IMS, *Rev. Geophys.*, 20, 531, 1982

¹³ McHenry, M.A., and R.C. Clauer, Modeled Ground Magnetic Signatures of Flux Transfer Events, *J. Geophys. Res.*, 92, 11,231, 1987.

The FTE was approximated as a cylinder with its axis directed along the constant uniform magnetic field (see Figure 3-4). Perturbation electric and magnetic field were found for current distributions corresponding to simplified models of FTE: one with an asymmetric current system suggested by Southwood (1985,1987)¹⁴, representing an isolated flux tube moving through the ambient medium, and the other one with a axially symmetric current system postulated by Saunders et al. (1984)¹⁵ and Lee (1986)¹⁶ responsible for the helical magnetic fields observed at the magnetospheric ends of FTEs.

Satellite measurements of electric fields expected during an encounter with an FTE depend on the parameters for the model and the relative motions of the FTE and the satellite. Figures 3-5 and 3-6 show 2 components of the electric field predicted for the satellite passing in the vicinity of an FTE footprint with an asymmetric current (Figure 3-5) and symmetric current distribution (Figure 3-6). In case of an asymmetric current system satellite crossing through the center of the structure would measure "double vortex" signature, while satellite "glancing" the flux tube would measure the bipolar signature in the electric field component aligned with the satellite motion. In case of the symmetric current system perturbation field is confined to the interior of the flux tube and corresponds to a "single vortex" signature. In the case of constant ionospheric conductivity and a field inclination close to 90°, the magnetic field signature should be out of phase by 90° with respect to the electric field. One should expect that the transverse magnetic field component should follow the electric field component measured along the direction of the satellite motion.

Particle fluxes associated with FTEs at ionospheric altitudes will depend on the time and

¹⁴ Southwood, D.J., Theoretical Aspects of Ionosphere-Magnetosphere-Solar Wind Coupling, *Adv. Space Res.*, 5, 7, 1985.

Southwood, D.J., The Ionospheric Signature of Flux Transfer Events, *J. Geophys. Res.*, 92, 3207, 1987.

¹⁵ Saunders, M.A., C.T. Russell, and N. Sckopke, Flux Transfer Events - Scale Size and Interior Structure, *Geophys. Res. Lett.*, 11, 131, 1984

¹⁶ Lee, L.C., Magnetic Flux Transfer at the Earth's Magnetopause, in *Solar Wind - Magnetosphere Coupling*, edited by Y. Kamide and J.A. Slavin, p.297, Terra Scientific, Tokyo, Japan, 1986.

location of observation. Shortly after the merging between closed magnetospheric field line and magnetosheath open line, one should expect to see the mixture of the hot magnetospheric particles and cold magnetosheath particles. Indeed, this is indicated by observations near the magnetopause. Since, however, the bounce time of magnetospheric particles is less than the Alfvén travel time, the magnetospheric particles will escape before electromagnetic signatures of FTE could be established at the ionospheric altitudes. Subsequently one should detect cold magnetosheath particles which have an easy access to ionospheric altitudes as the flux tube convects at cusp latitudes. Later on, when magnetosheath plasma accelerates to supersonic levels, its access to the low-altitudes is inhibited, and one may expect to detect polar rain levels.

In order to test predictions of this simple model we presented results of a search through the available S3-2 data for electric and magnetic field signatures from the mid-day sector displaying irregular structures of scales 100 to 200 km, consistent with ionospheric mapping of FTEs. Approximately 40 passes of S3-2 between December 1975 and April 1976 were reviewed. An event selected for detailed analysis was observed approximately at 2219 UT on January 5, 1976 during an equatorward crossing of the northern dayside auroral region at about 1030 MLT. The qualitative electric and magnetic field fluctuations expected during a satellite encounter with an FTE at ionospheric altitudes are compared with single component measurements for S3-2. Although an encounter with a fast stream in a plasma flow poleward of the cusp cannot be excluded, the data are consistent with expectations for the S3-2 spacecraft having made a near center crossing of an ionospheric footprint of an FTE with a diameter of about 150 km moving eastward along the polar cap boundary with a velocity of 1.3 km/s (see Figure 3-7).

3.4 Field and Particle Characteristics in DE-2 Crossings of the Low Cusp/Cleft Regions

In collaboration with Drs. Nelson Maynard and William Burke a comparative analysis of DE-2 field and plasma measurements was undertaken at times that the satellite was crossing dayside cusp/cleft regions. This is done with an objective to identify transient and steady-state electrodynamic phenomena coming from the dayside magnetopause, low-latitude boundary layer and plasma mantle. High, variable fluxes of soft electron precipitation, intense fluctuations in electric fields and field-aligned currents may provide source of free energy for generating density irregularities within the ionospheric F-layer. Satellite measurements reflect superposition of distant processes coupled to the magnetopause boundary layers and local ionospheric phenomena.

After an initial data selection and development of computer programs to handle diverse data sets, our current research is concentrating on: i) analysis and interpretation of large, variable fields at the equatorward boundary of the cusp (see section below); ii) comparison of high resolution electric and magnetic field data for the dayside crossings (work in progress) and iii) dynamics of the cusp during the large storm of September 6, 1982 (work in progress).

3.4.1 Intense Electric Fields at the Equatorward Boundary of the Dayside Cusp

Intense electric fields with scale down to 1 km are occasionally detected by the VEFI double probe instrument on board the DE-2 satellite at the equatorward boundary of dayside cusp precipitation (Maynard, 1985)¹⁷. They are collocated with the sharp onset of the broad-band electrostatic noise in the ULF-ELF band and occur for the IMF B_z southward. Analysis of these type of events may elucidate processes coupling the dayside magnetopause boundary layers to the ionospheric cusp/cleft regions. We concentrated on data measured

¹⁷ Maynard, N.C., Structure in the DC and AC Electric Fields Associated with the Dayside Cusp Region, in *The Polar Cusp*, edited by J.A. Holtet and A. Egeland, D. Reidel, Hingham, MA, p.305, 1985.

on September 6 1982 during the large magnetic storm. K_p values during this day were very high reaching 8 and 9. The strong ring current developed during the day with the DST index reaching approximately 300 nT in the middle of the day. Solar wind density and velocity were variable with high values during the most of the day.

DE-2 measurements indicate presence of large, highly variable electric fields and magnetic fields, intense fluxes of low-energy electrons, energy dispersion in ion fluxes, increased electron temperature and variable electron plasma densities. In Publication 9 we present comparison of high altitude data from DE-1 indicating that the DE-1 satellite entered the magnetosheath for a short period, approximately 20 minutes after the low-altitude DE-2 satellite passed through the southern hemisphere cusp. In what follows we will summarize low-altitude DE-2 measurements obtained during this period. Problems relating high and low altitude observations are discussed in detail in the Publication 9 with the objective of identifying low-altitude signatures of the magnetopause under strongly driven conditions with IMF B_z south, conditions favorable for magnetic merging.

Figures 3-8 and 3-9 present detailed comparison of plasma and field characteristics for a satellite pass through the southern polar cusp region at 8:37 UT. One can notice that the region of highly variable equatorward directed electric fields (corresponding to an eastward convection) is collocated with high fluxes of soft electrons. There is a dispersion in ion energy with energy decreasing poleward of the equatorward boundary of this region. Pitch angle distribution of energetic electrons abruptly changes from trapped to isotropic. There is an intense spike-like electric field signature collocated with the boundary indicated by particle characteristics. Ambient plasma density (not shown here) increases rapidly poleward of the particle boundary. Figure 3-9 presents electric field measurements and deviations of

magnetic field measurements from the reference field in the satellite coordinate system, where x is aligned with the orbital motion of the satellite, y is directed upwards, and z is directed eastward. In this coordinate system positive slopes in B_z represent field-aligned currents into the ionosphere, negative slopes - currents out of the ionosphere. There are large scale currents in region A (into the ionosphere) and in region B (out of the ionosphere). Small scale features are superposed on top of this large scale system. Assuming that the sharp boundary in the particle characteristics corresponds to the boundary between open and closed field lines leads to the conclusion, that large scale field-aligned current system is on open field lines and can be interpreted as the system of the cusp currents. Comparing E_x and B_z one can notice, that they are not well correlated as would be expected for the satellite crossing the system of multiple small scale field-aligned current sheets in the sunlit ionosphere. In particular, the spiky equatorward electric field at the boundary between region B and C doesn't have a counterpart in B_z . Figure 3-10 shows 6 seconds of data at this boundary. To the both sides of the shaded region E_x seems to track B_z quite well leading to a conclusion that the data are consistent with an interpretation as field-aligned currents closed by the ionospheric Pedersen currents with an integrated Pedersen conductivity of several mhos. This interpretation does not hold within the shaded region. We postulate that these km scale variations of essentially electrostatic origin are caused by ionospheric processes.

Our scenario is presented in the Figure 3-11 invoking an idea of the convection gap (Moses et al. 1988¹⁸, Crooker 1988)¹⁹. DE-2 satellite moving equatorwards encounters region of eastward convection and crosses the ionospheric projection of the merging line at

¹⁸ Moses, J.J., G.L. Siscoe, R.A. Heelis and J.D. Winningham, A Model for Multiple Throat Structures in the Polar Cap Flow Entry Region, *J. Geophys. Res.*, 93, 9785, 1988.

¹⁹ Crooker, N.U., Mapping the Merging Potential from the Magnetopause to the Ionosphere Through the Dayside Cusp, *J. Geophys. Res.*, 93, 7338, 1988.

the boundary between region B and C. The poleward spike at 8:37:39.2 can be interpreted as the ionospheric signature of a merging event at the magnetopause. This interpretation is consistent with a balance of forces acting on freshly reconnected field line (Cowley et al. 1983)²⁰. The force with which magnetosheath plasma drags merged flux tubes in the direction of its local flow will cause an initial motion of merged flux tubes, in our case, towards the dawn. Later on, when the force due to the magnetic tension will dominate, plasma will start moving towards the dusk, as expected in the southern hemisphere for IMF B_y positive. Field signatures within the shaded region can be understood in terms of local ionospheric processes. Large fluxes of soft electrons precipitate to the F-region causing enhanced ionization with the sharp density gradient at the precipitation boundary (coincident with the ionospheric projection of the merging line). In the presence of the convection velocity component directed in the same direction as density gradient, the equatorward boundary of the plasma enhancement is unstable to the growth of ExB instability leading to plasma density irregularities. These in turn set up polarization electric fields, which would show up in satellite measurements as variable electric fields decoupled from magnetic field variations. Non-linear cascading processes produce higher frequency turbulence and contribute to ULF-ELF activity observed poleward of the boundary between open and closed field lines. Density irregularities at the boundary would smear out the initial density gradient if it were not for the fact that there is a continuous source of soft electrons enhancing ionization of the F region plasma and maintaining the gradient. One may expect, that the turbulence created on the plasma gradient along the equatorward boundary of the cusp might evolve in such a way as to appear as a standing wave, similar to the standing turbulence encountered

²⁰ Cowley, S.W.H., D.J. Southwood and M.A. Saunders. Interpretation of Magnetic Field Perturbations in the Earth's Magnetopause Boundary Layers, *Planet. Sp. Sci.*, 31, 1237, 1983

by the rafters on a river.

3.5 An Equation for Field-Aligned Current

The current flow between the magnetosphere and the ionosphere is one manifestation of magnetosphere-ionosphere coupling. Small scale currents flow between the magnetosphere and ionosphere within and adjacent to auroral arcs. The upward currents within the arcs are carried by energetic precipitating electrons. The arc is the visual signature of the energy deposited in the thermosphere by these electrons.

One mechanism which has been proposed to explain the creation of auroral arcs is the adiabatic acceleration of magnetospheric electrons through a field-aligned electrostatic potential. The upward field-aligned current which results is a function of the density and the parallel and perpendicular temperatures of the magnetospheric electron population as well as the magnitude and altitude of the electrostatic potential drop. Brüning and Goertz²¹ gave an equation for the field-aligned current carried by a an adiabatically accelerated bi-Maxwellian electron distribution. They assumed that the field-aligned electrostatic potential drop through which the electrons travel obeys Fridman and Lemaire's criterion²². Brüning and Goertz discussed how the current varies with the altitude of the top of the potential drop. Their Figure 4 indicated that, depending on the anisotropy of the electron distribution function, a maximum or minimum in the field-aligned current will occur as the altitude of the top of the potential drop varied.

We have shown that their equation is incorrect²³. In fact, for potentials which obey

²¹ Brüning, K. and C. K. Goertz, Influence of the electron source distribution on field-aligned currents, *Geophys. Res. Lett.* **12**, 53-56, 1985

²² Fridman, M. and J. Lemaire, Relationship between auroral electron fluxes and field-aligned electric potential difference, *J. Geophys. Res.* **85**, 664-670, 1980.

²³ Greenspan, M. E., Origins of enhanced field-aligned current at the edge of an auroral arc, *J. Geophys. Res.* **94**, 12,037-12,042, 1989

Fridman and Lemaire's criterion, local extrema cannot exist in the field-aligned current considered as a function of the altitude of the top of the potential drop. The field-aligned current which reaches the ionosphere increases monotonically as the altitude of the top of the potential drop increases. This is because, as the altitude of the top of the potential drop increases, more and more earthward-moving electrons are accelerated into the expanded loss cone before they reverse direction because of magnetic mirroring. For a bi-Maxwellian electron distribution that originates at B , with temperatures T_{\parallel} and T_{\perp} and falls adiabatically through a potential drop which begins at $B_{v\parallel}$, the corrected equation is given by:

$$j_{\parallel} = en \left[\frac{T_{\parallel}}{2\pi m} \right]^{1/2} \left[\frac{\gamma\alpha}{(\alpha + \beta - 1)} \right] \left\{ 1 - \left[\frac{(\gamma - \beta)}{(\gamma + \alpha - 1)} \right] \exp \left[\frac{-\chi(\alpha + \beta - 1)}{(\gamma - \beta)} \right] \right\} \quad (5)$$

Here, $\alpha = T_{\parallel}/T_{\perp}$, $\beta = B_{v\parallel}/B_s$, $\gamma = B_I/B_s$, and $\chi = e\Phi/T_{\parallel}$. Because some backscattered electrons will be produced with $E > \mu B_{v\parallel}$, so that they can surmount the potential barrier and reach the magnetosphere, equation gives an upper limit on the net upward field-aligned current.

Equation 5 is plotted in Figure 3-12. The quantity $en[T_{\parallel}/(2\pi m)]^{1/2}$ has been set equal to one, $\gamma = 50$, and $\chi = 3$. The current $j_{\parallel}(\beta)$ is shown for $\alpha = 5, 1$, and 0.2 . Figure 3-12 illustrates the absence of local extrema in the magnitude of the current density and shows that for parameters typical of the magnetosphere, the current density is proportional to alpha.

Rocket and radar observations of auroral arcs indicate that upward field-aligned currents associated with such arcs sometimes are larger at their edges than within the arcs. Brüning and Goertz reported one such set of observations, made by instruments on the Porcupine F4 rocket. Porcupine F4 measured a fourfold increase in the magnitude of the upward field-aligned current at the edge of an auroral arc over its value in the arc's center, while the

energy of the peak in the electron differential flux decreased at the edge of the arc and the electron distribution function remained nearly isotropic in pitch angle throughout the arc.

Brüning and Goertz attempted to explain the increase in current at the edge of the arc as an effect of an increase in the altitude of the top of the potential drop at the edge of the arc. Our work shows that if the arc traversed by Porcupine F4 was created by adiabatic acceleration of magnetospheric electrons, the increase in upward current at the edge of the arc cannot be explained solely by an increase in the altitude of the top of the field-aligned potential drop. The fact that the electrons seen at the rocket were nearly isotropic in pitch angle means that, if the electrons were accelerated adiabatically, the top of the potential drop was well above the ionosphere throughout the acceleration region. Thus, an increase in the density, a decrease in the perpendicular temperature of the magnetospheric electron population, or both must occur at the edge of the arc to explain the observed increase in upward field-aligned current.

3.6 Collaborative Studies of Ionospheric Signatures of Magnetospheric Boundary Regions

The question of identifying ionospheric signatures of magnetospheric boundary regions recently has received considerable attention. The first Geospace Environment Modeling (GEM) observing workshop, "Ionosphere Signatures of Cusp, Magnetopause, and Boundary Layer Processes," was held at the University of Maryland in October of 1989. Participants in the workshop agreed that identification of ionospheric signatures of the magnetopause and boundary layers in ground-based data should be a primary goal of the first GEM observing campaign. They further agreed that intercalibration of ground signatures with satellite observations as the spacecraft flew over the ground stations could be a vital aid in achieving this goal.

Regis College personnel have been collaborating with scientists who operate ground-based high-frequency radars in an effort to achieve such intercalibration of velocity measurements from the DMSP drift meter and from the Halley Bay coherent-scatter radar. Coherent scatter radar can directly measure only the line-of-sight component of the plasma velocity. Various techniques are used to infer two dimensional velocity patterns from a set of such measurements taken for different beam directions²⁴. DMSP F9 drift meter measurements have been used to confirm the two-dimensional convection pattern inferred within the Southern Hemisphere cusp between 1346 and 1349 UT on October 10, 1988. The satellite orbit was nearly parallel to the line-of-sight of one of the radar beams. Figure 3-13 shows the DMSP horizontal drift data and the drift velocity transverse to the radar beam determined from Halley Bay radar data. The more direct satellite horizontal velocity measurement and the velocity transverse to the beam calculated from the radar data show good agreement. Both the drift meter and radar data show greater than usual turbulence within the cusp region²⁵.

²⁴ Ruohoniemi, J. M., R. A. Greenwald, D. B. Baker, J.-P. Villain, C. Hanuise, and J. Kelly, Mapping high-latitude plasma convection with coherent HF radars, *J. Geophys. Res.* 94, 13463-13477, 1989.

²⁵ Baker, K. B., R. A. Greenwald, J. M. Ruohoniemi, J. R. Dudeney, M. Pinnock, P. T. Newell, and M. E. Greenspan, Simultaneous HF-radar and DMSP observations of the cusp, submitted to *Geophys. Res. Lett.*, 1990.

PROJECTED ELECTRIC FIELDS
DAY 82051

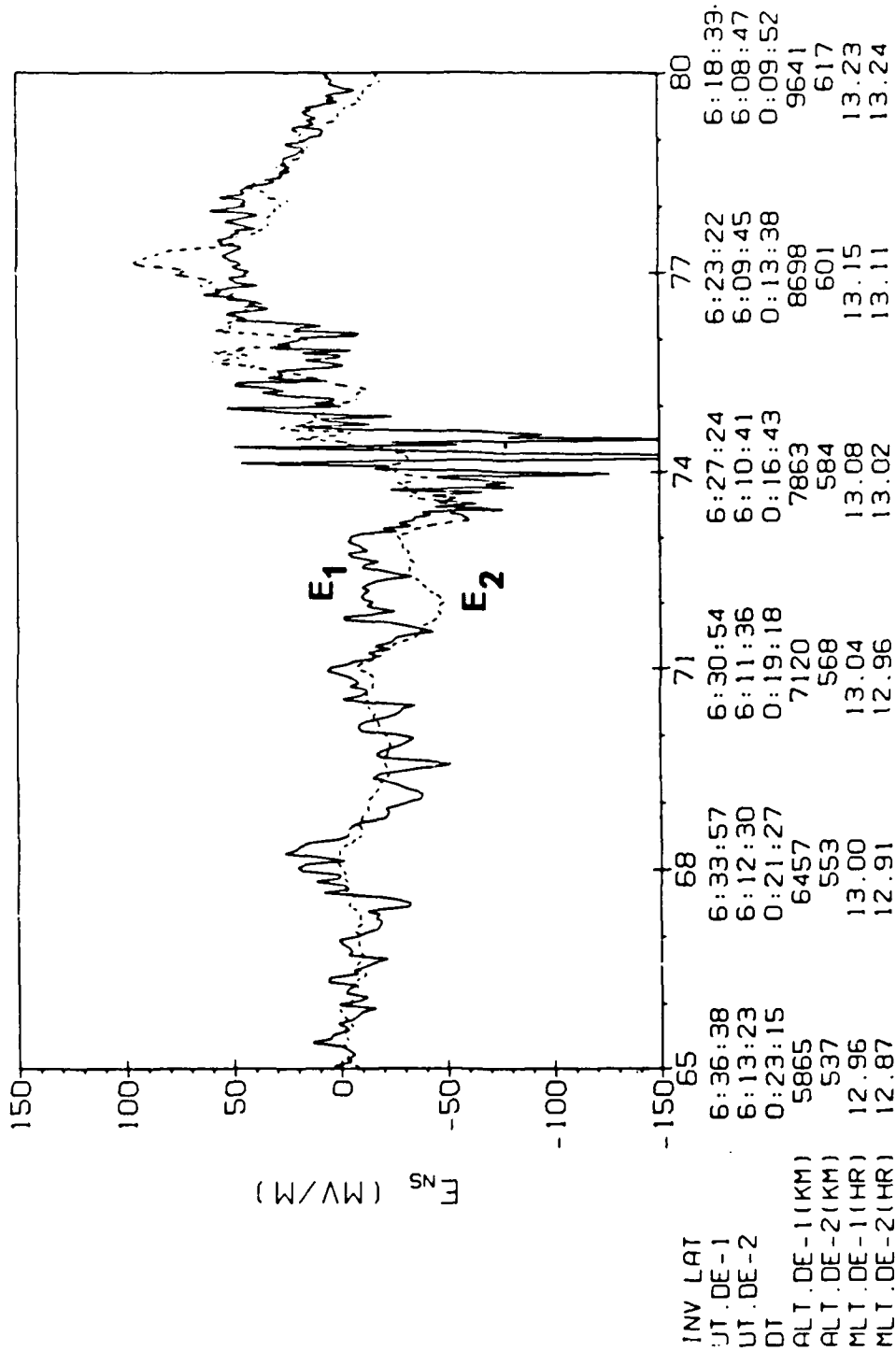


Figure 3-1 North-south electric fields measured with DE-1 (solid line) and DE-2 (dashed line) near a junction on day 51 of 1982. These data show a similar oscillatory structure between 65 and 73 degrees invariant latitude, even though they passed through the region at different times. Similar oscillations were present in the magnetic fields, indicating that the field-aligned current consisted of alternating bands of up and downward current.

$$G = 10^{-8} \text{ mho/m}^2 \quad \Sigma_p = 4.6 \text{ mho} \quad \Sigma_g = 3.66 \text{ mho} \quad V_{||}(0) = -120 \text{ volts}$$

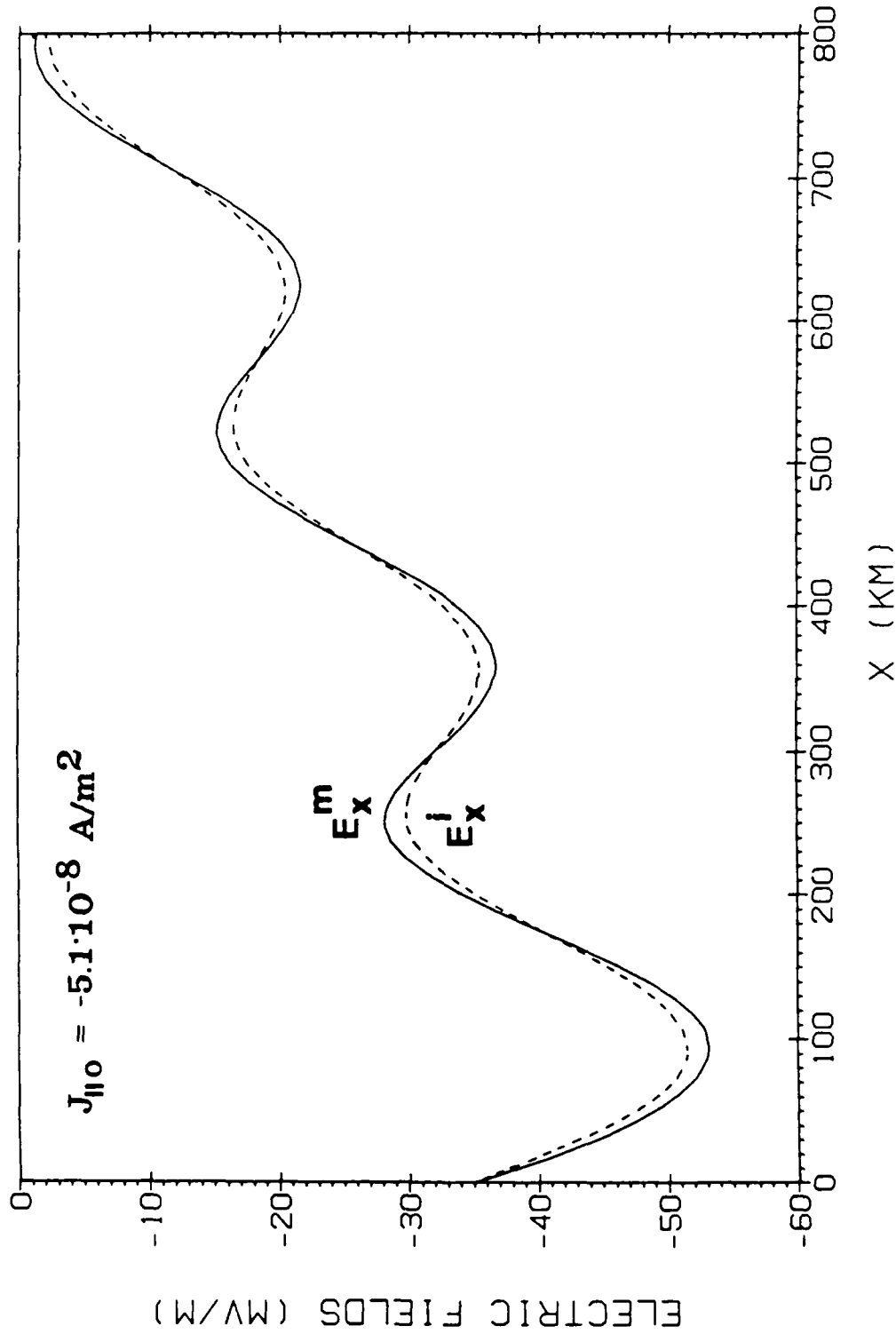
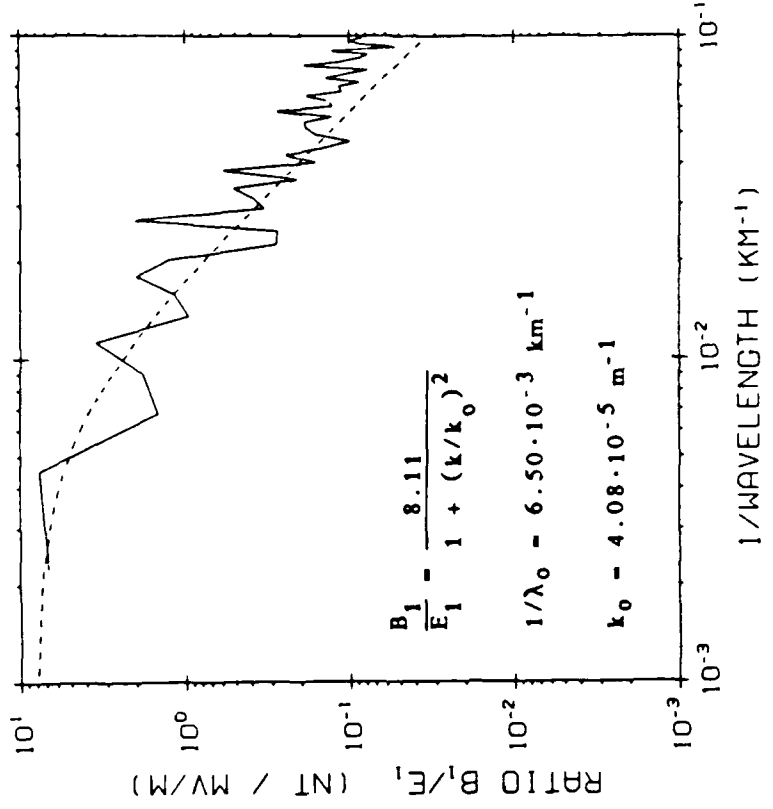


Figure 3-2 Electric fields calculated with a numerical model, using values appropriate to the oscillation event which was detected with the DE satellites.

65° - 69° INV. LAT.



65° - 69° INV. LAT.

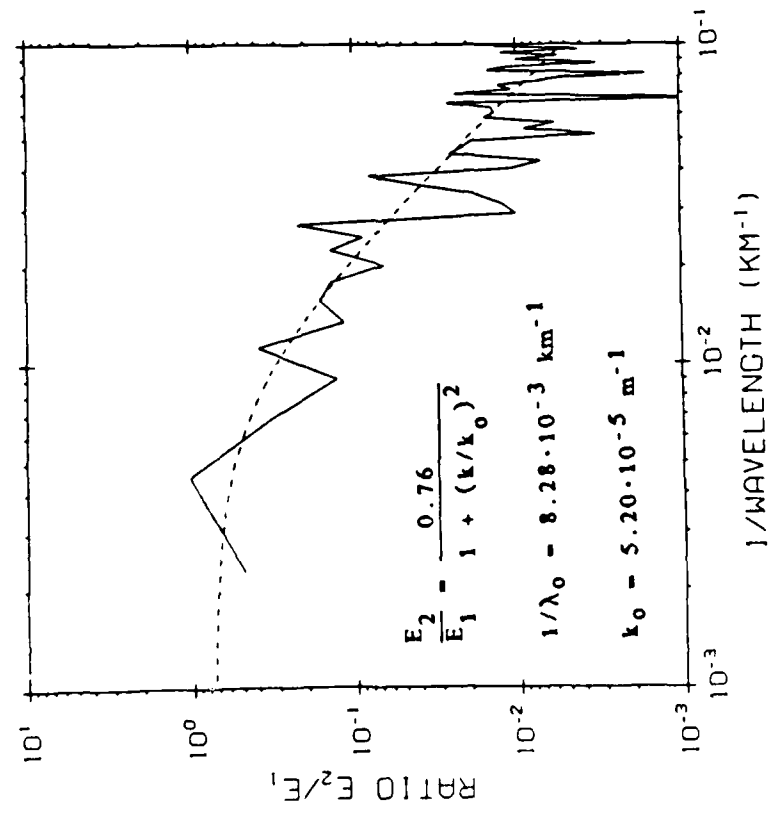


Figure 3-3 Example which demonstrates measurement of magnetic field line conductivity, on the basis of the ratio of electric or magnetic field magnitudes. The graph on the left shows the ratio of electric fields at low and high altitudes (from DE-2 and DE-1) as a function of frequency, as determined by Fourier transforms. The graph on the right shows the ratio of the magnetic field to electric field at high altitude (DE-1). The dashed lines show the equations which were determined to be the best fit to the data, from which the field line conductivity is calculated.

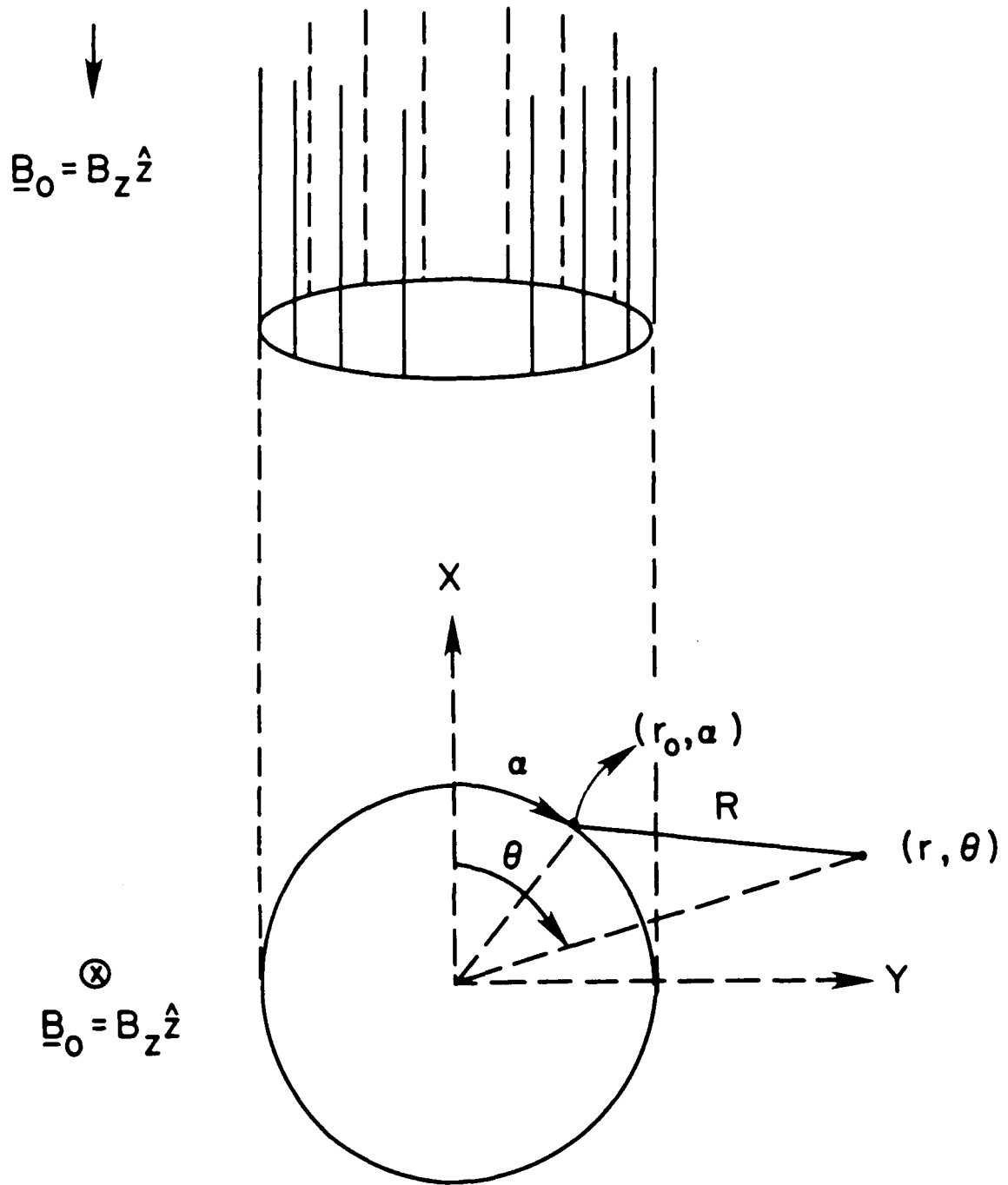


Figure 3-4 (a) An FTE modeled as a cylinder with its axis along the ambient magnetic field B_0 . (b) Cross section of an FTE in the plane perpendicular to its axis.

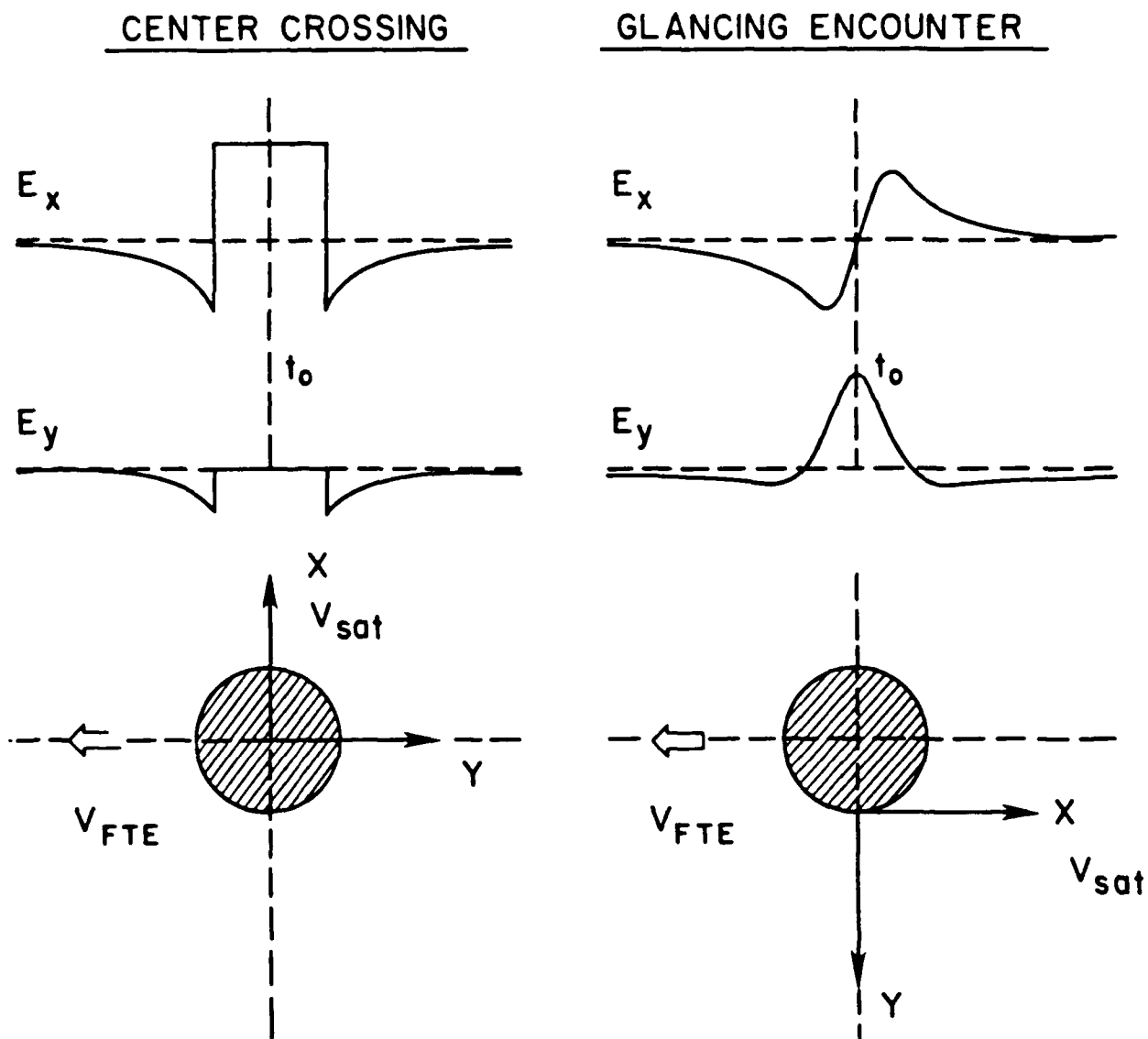
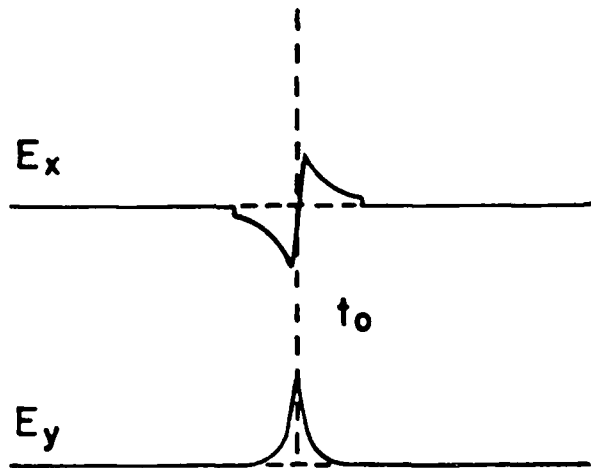


Figure 3-5 Electric field signatures predicted for the model with an asymmetric current distribution as should be measured (a) by the satellite passing through the center of the FTE and (b) during the grazing incident encounter. E_x and E_y are presented in the satellite coordinate system, where x-axis is directed along the satellite motion and y-axis is perpendicular to the orbital track. These figures were made using arbitrarily selected parameters: $V_{FTE} = 2$ km/s and $V_{sat} = 7.5$ km/s.

NEAR CENTER CROSSING



GLANCING ENCOUNTER

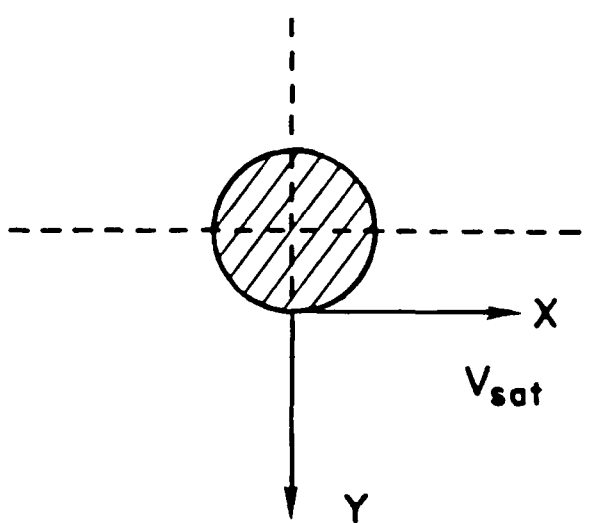
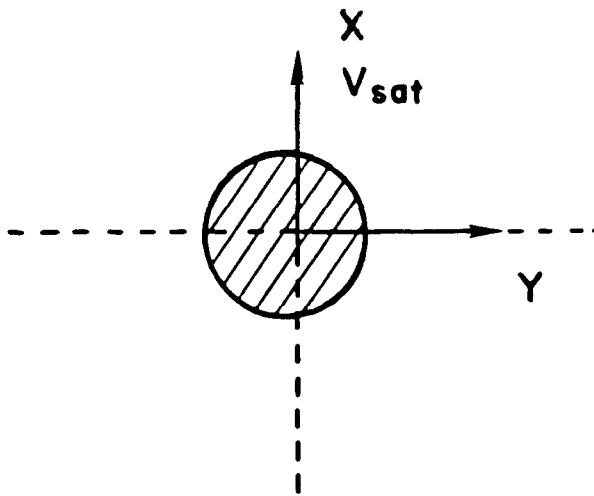
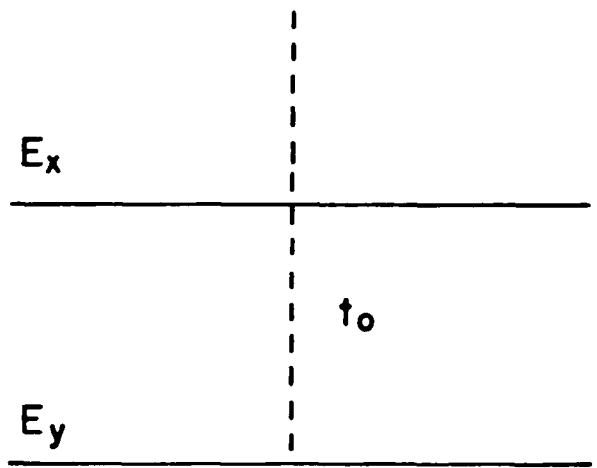


Figure 3-6 Same as Figure 3-5 for the symmetric current distribution. Figure 3-5 (a) presents electric field signatures as should be measured by the satellite passing close to the center of the symmetric FTE.

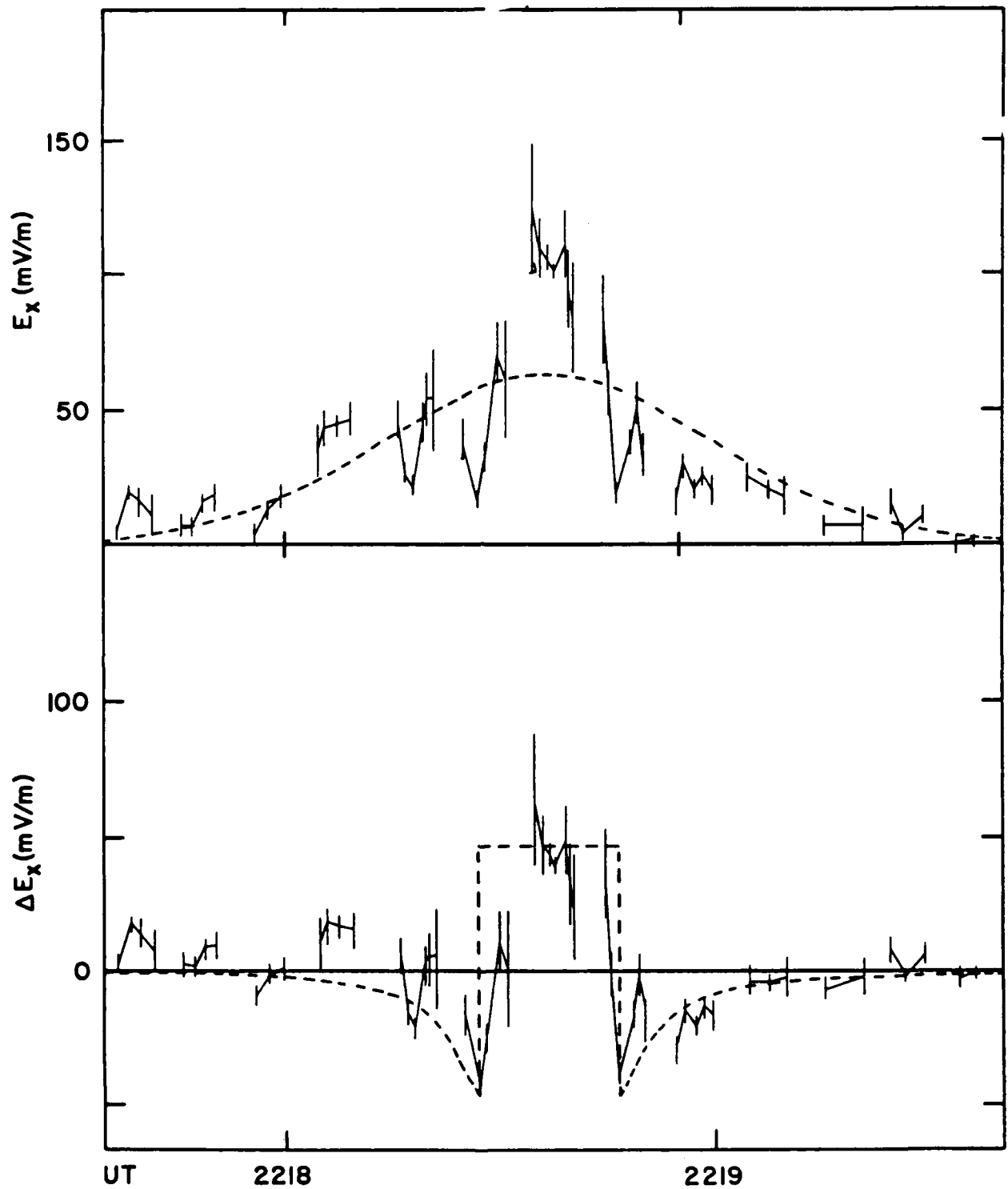


Figure 3-7 Comparison of S3-2 electric field measurements with the predictions of the model with an asymmetric current distribution. The upper panel shows E_x , the electric field measured along the satellite orbital motion. The broken line represents an assumed, unperturbed background electric field approximated by a Gaussian. Comparison of the model predictions with E_x , the residual electric field measurements after subtraction of the Gaussian background is shown at the lower panel. The model parameters are: $V_{sat} = 7.5$ km/s, $V_{FTE} = 1.3$ km/s.

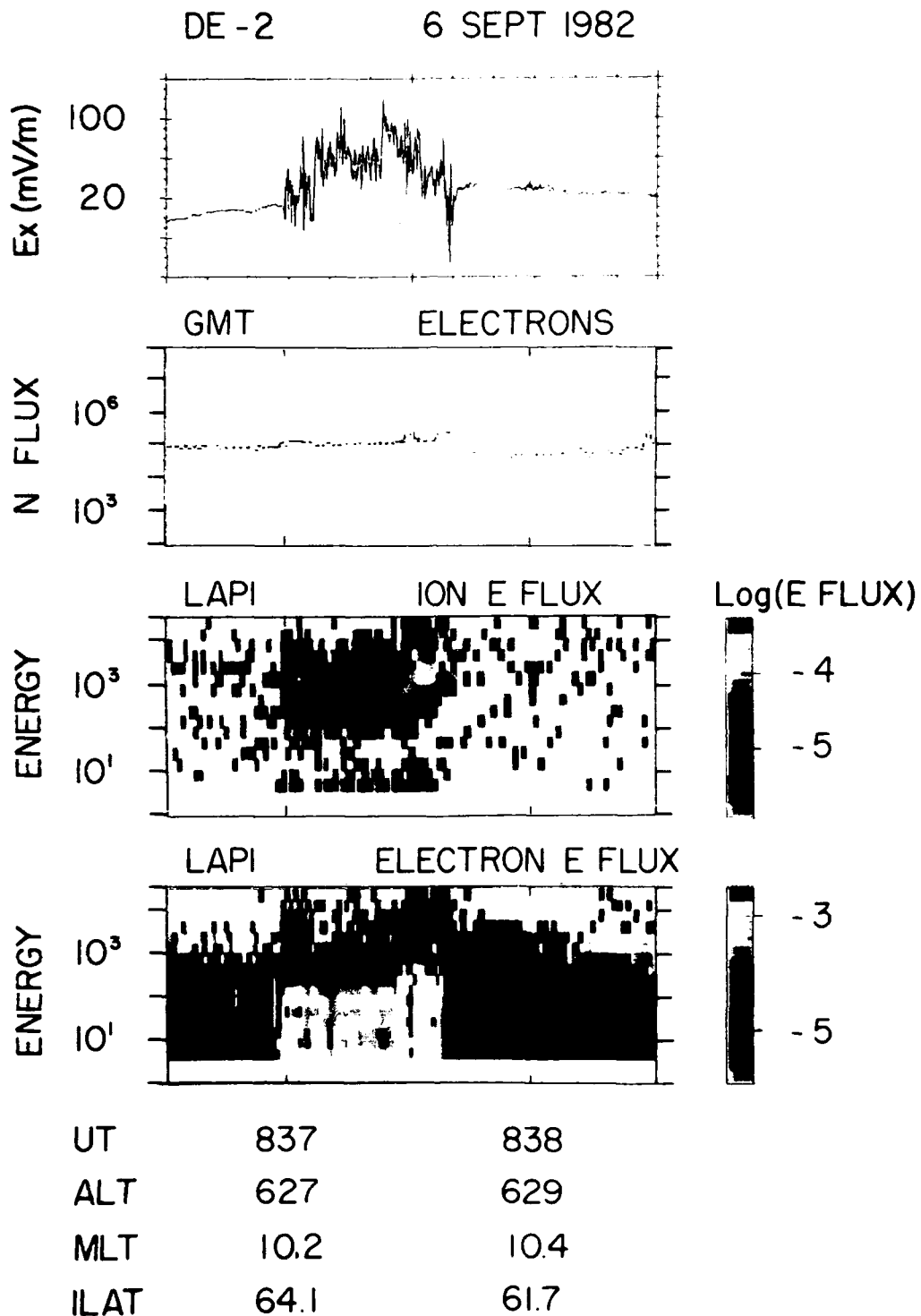
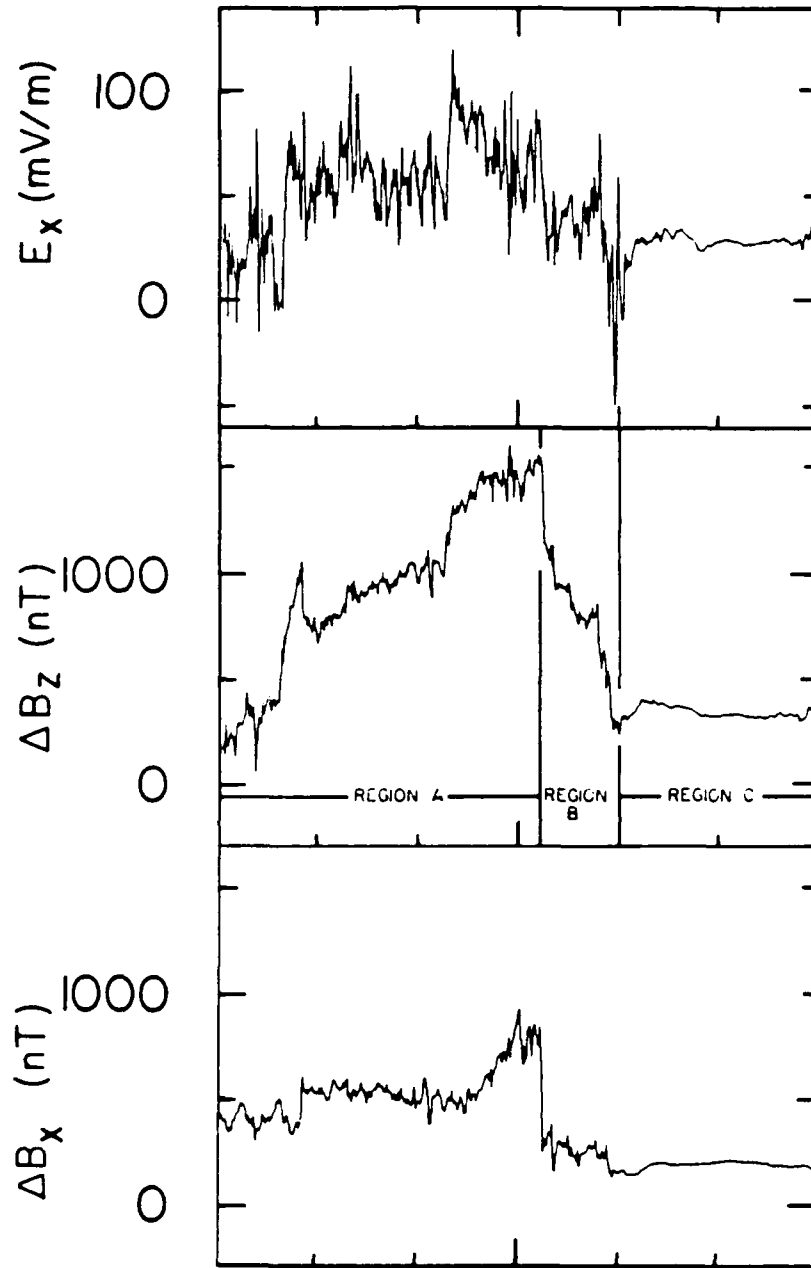


Figure 3-8 Directional, differential energy fluxes of soft electrons (bottom panel) and ions (second from bottom panel) measured by the LAPI instrument on DE-2 plotted as functions of time. The electron and ion spectrometers looked at pitch angles near 14° and 6° , respectively. The second panel from the top gives the number flux of energetic electrons (>35 keV) as measured by the Geiger tubes with pitch angles near 0° and 90° . The electric field measurements in the top panel represent the component positive in the direction of the satellite motion.

DE -2 6 SEPT 1982



837	UT	838
622	ALT	629
10.2	MLT	10.4
64.1	ILAT	61.7

Figure 3-9 Components of magnetic perturbations along (bottom panel) and across (middle panel) the satellite orbital motion, plotted as functions of time. A positive slope in B_z indicates a field-aligned current into the ionosphere. The electric field data plotted in the top panel are the same as those in Figure 3-8.

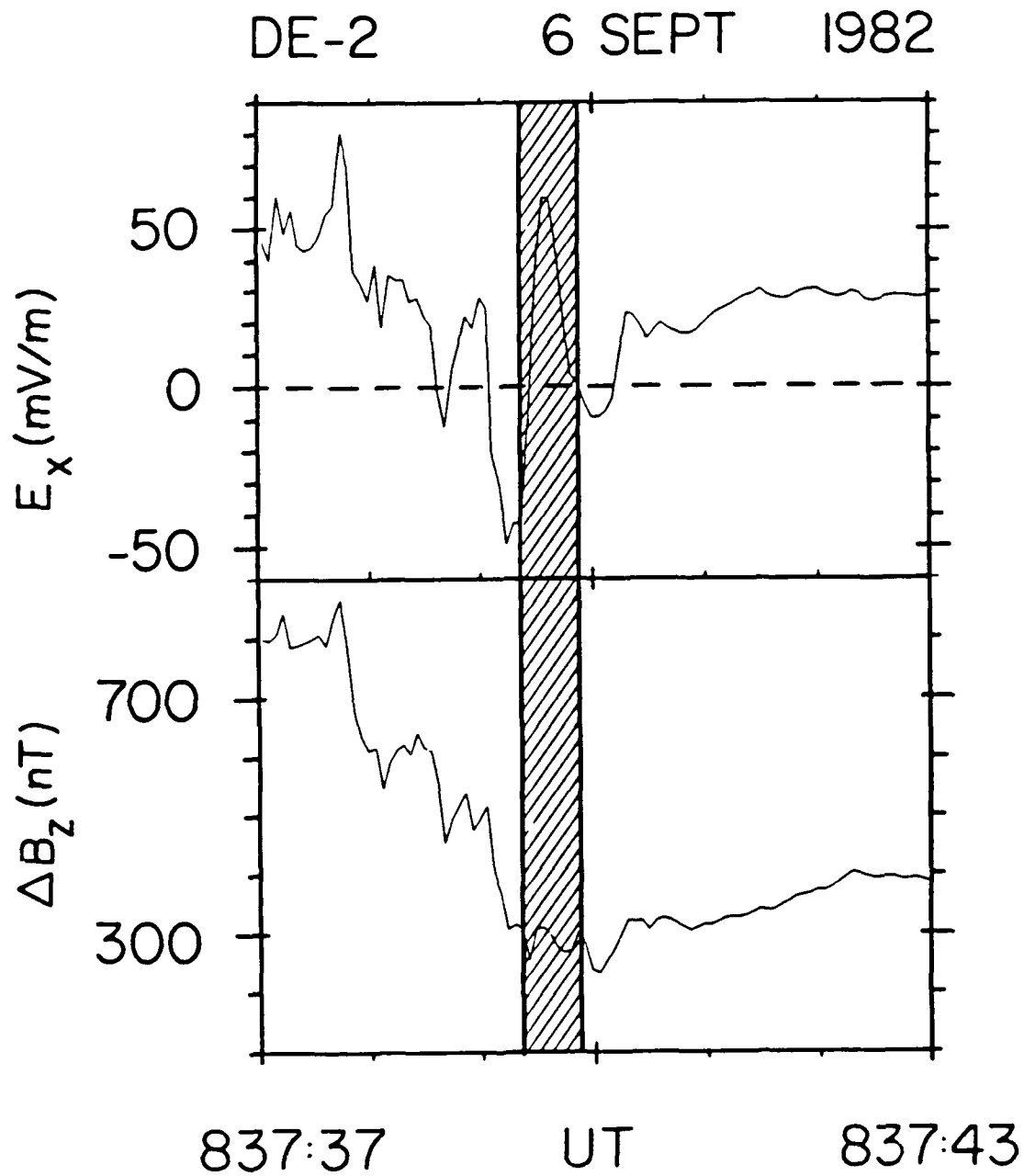


Figure 3-10 An expanded plot of the electric and magnetic field measurements taken during a six second period as the DE-2 satellite crossed the sharp boundary in the particle characteristics.

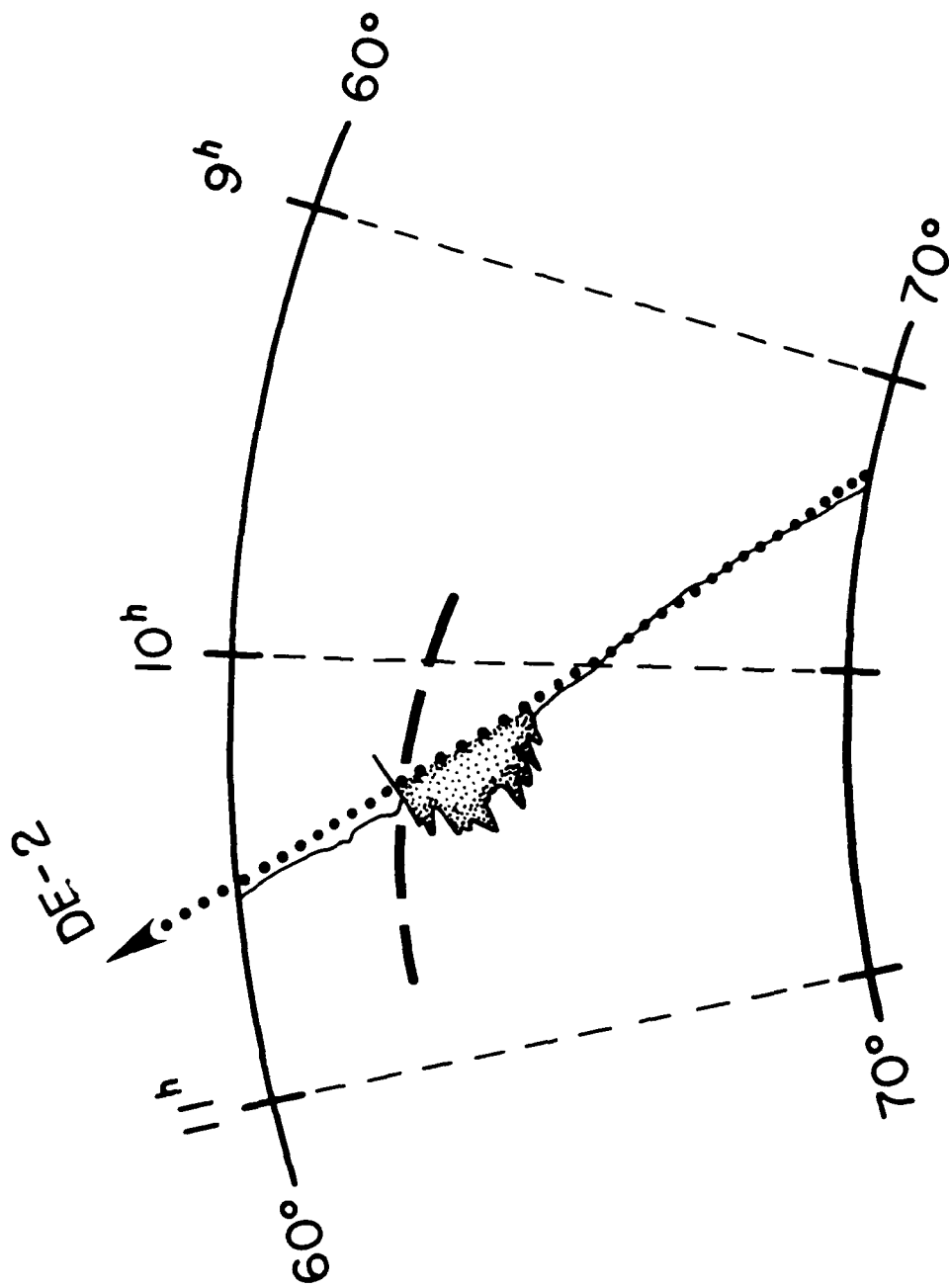


Figure 3-11 Trajectory of DE-2 in magnetic local time and invariant latitude. The electric field measurements are used to represent the location and direction of ionospheric plasma flow. The shaded region marks the extent of soft electron precipitation. The location of the "gap" or ionospheric projection of the merging line appears as a thick, broken line oblique to the satellite trajectory and plasma flow.

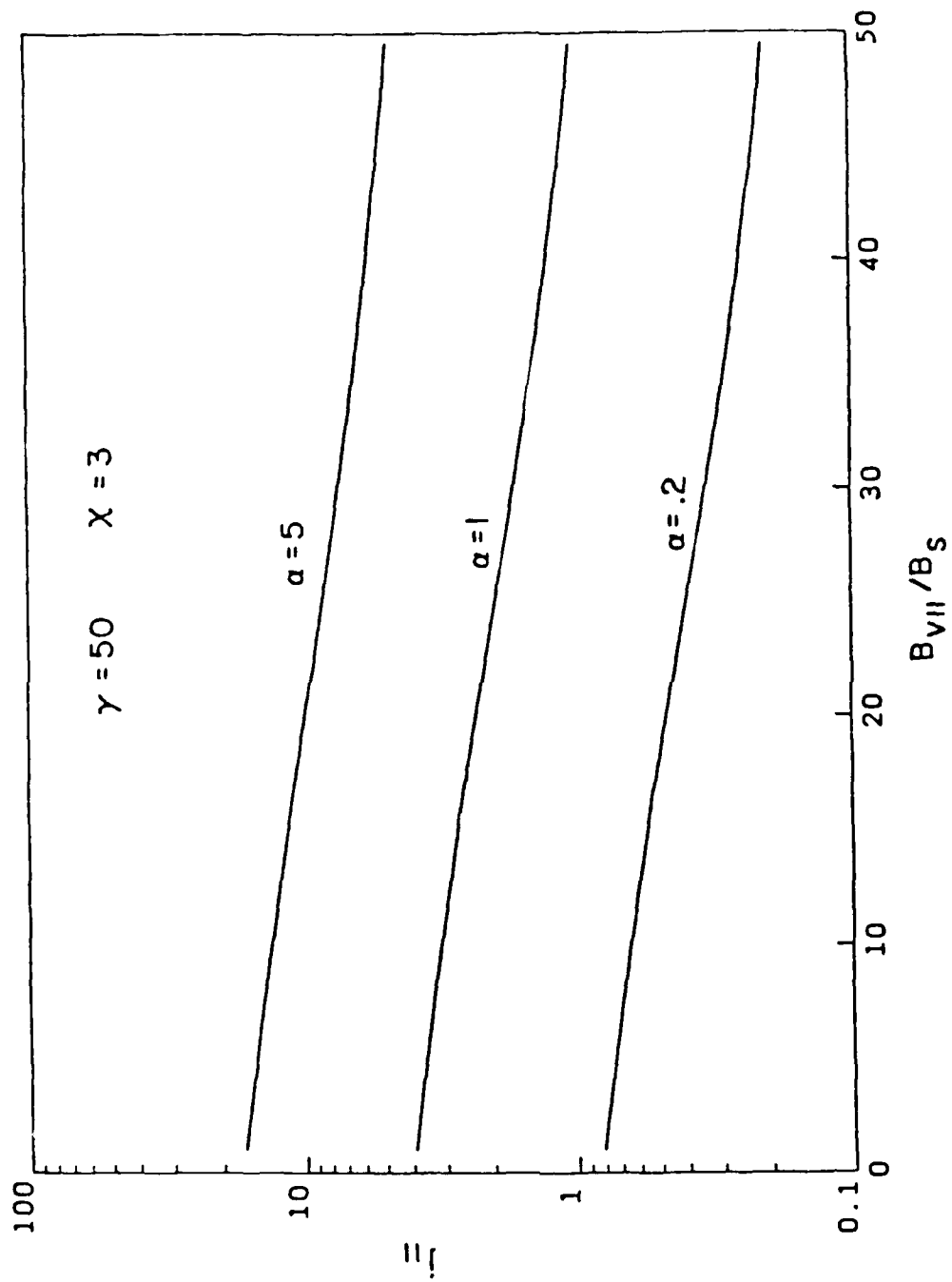


Figure 3-12 Dependence of field-aligned current density at the ionosphere on $\beta = B_{v||}/B_s$.

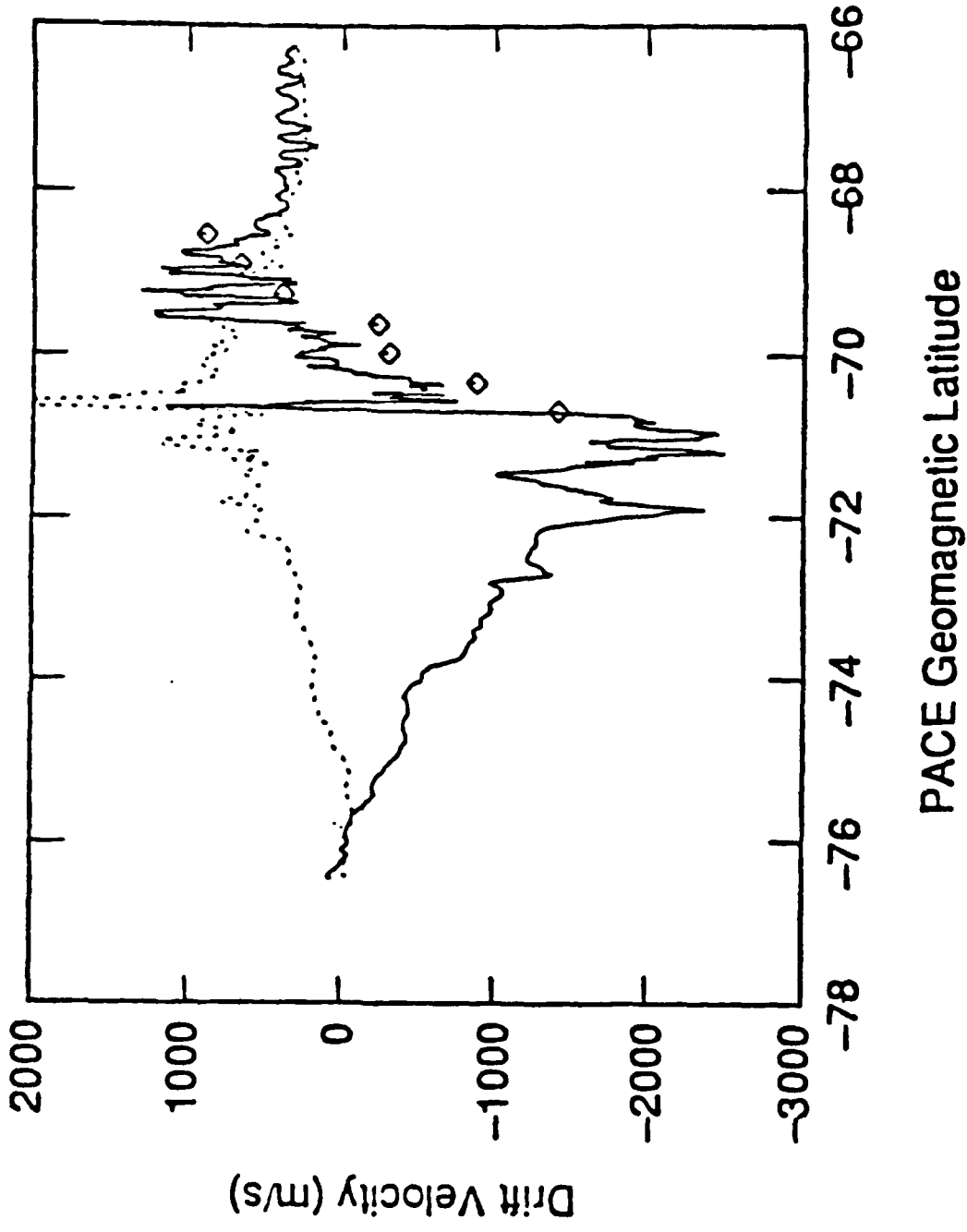


Figure 3-13 Comparison of the DMSP drift data and the drift velocity transverse to the Halley Bay radar beam as determined from the radar line-of-sight velocity data on October 10, 1988. The DMSP horizontal drift is indicated by the solid curve, while the vertical drift is indicated by the dotted curve. The radar data are indicated by the diamonds. Positive values are westward for the horizontal component or upward for the vertical component.

4. IONOSPHERIC PLASMA STUDIES

4.1 Midlatitude and Equatorial Ion Morphology at Solar Minimum

A study of the morphology of the thermal plasma ions measured by the DMSP F8 RPA during the solar minimum period July 1987 to December 1987 is in progress. The goals of this project are to characterize the variations in ion density and composition measured by the RPA and to see how these variations are related to ion drifts. Quiet, moderately active, and disturbed days shortly after the June solstice, near the September equinox, and shortly before the December solstice have been selected for study. To aid in comparing ion behavior at different longitudes during one day and on different days, a program was developed to plot ion density and composition versus magnetic latitude rather than time. Stack plots showing all the dawn or dusk orbits within a day versus magnetic latitude further facilitate the comparison process. Some stack plots have been drawn by hand, and a program to automate the creation of these plots now is being written.

Preliminary results show that densities less than 10^3 cm^{-3} occur in the winter hemisphere in both June and December during both the dawn and dusk legs of the orbit. Near solstice, light ions predominate in the winter hemisphere. Near the September equinox, light ions were observed near the equator at both dawn and dusk. In September at dawn, plasma flows toward the equator. Near the equator, the plasma flow is upward, and at the equator, the plasma flows westward with respect to the surface of the earth. Figure 4-1 illustrates these effects on September 19, 1987, which was a very quiet day. In September at dusk, longitude exerts a strong control over the total density and ion composition regardless of activity. This is not true at dawn. This result is not unexpected, because sunlight rather than energy input from the magnetosphere dominates dayside mid-latitude and equatorial

processes. When stack plots have been completed and analyzed for the nine days under study, density and composition measurements will be compared with the predictions of the International Reference Ionosphere.

4.2 Density Depletions Observed at 840 km During the Great Magnetic Storm of March 1989

During the great magnetic storm of March 13-14, 1989, the SSIES sensors on the DMSP F8 and F9 spacecraft detected in-situ ion density levels which may represent large depletions in the ion density at 840 km altitude near the equator. W. J. Burke of the Air Force's Geophysics Laboratory, C. E. Rasmussen of Utah State University, and M. E. Greenspan of Regis College have begun a study of these anomalous in-situ densities. A preliminary report was presented as a contributed paper at the Fall, 1989 AGU meeting.

The DMSP F8 spacecraft observed these depletions at local dawn on March 13, during orbits which crossed the equator at 1346 UT, 1528 UT, and 1710 UT at geographic longitudes of 248°E, 222°E, and 196°E. Unfortunately, DMSP F8 data are missing from 1705 UT to 2110 on March 13. F9 measured depletions at 2130 LT during orbits which crossed the equator at 0050 and 0232 on March 14 at 309° and 284° east longitude. On March 14, 1989, F8 again observed depletions at dusk on March 14 during two orbits which crossed the equator at 1149 UT and 1322 UT at 278°E and 251°E.

Figure 4-2 shows the most dramatic of the depletions, detected by F9 shortly after midnight on March 14, 1989. The density dropped by a factor of 50 over a distance of 170 km as opposed to more typical conditions as shown in Figure 4-3. The depletion in density extends over 4000 km of the satellite orbit, from a magnetic latitude of 9° to a magnetic latitude of -16°. The spacecraft entered the depletion at a magnetic longitude of 25° and left

it at a magnetic longitude of 13° . The mechanisms which caused the depletions and which maintained the very large gradients in plasma density at the edges of the depleted regions are under investigation.

The two depletions detected by DMSP F9 were accompanied by large plasma drifts directed westward with respect to the surface of the earth and upward. The westward drifts reached amplitudes of nearly 400 m/s, and the upward drifts 250 m/s. Large westward drifts with respect to the surface of the earth also accompanied the depletions seen by DMSP F8, but they are not so clearly associated with large upward drifts. This suggests that these depletions may have formed east of DMSP F8's longitude and drifted to the spacecraft's meridian.

The depletion shown in Figure 4-2 occurred near the longitudes of the Fortaleza and Cachoeira Paulista ionosondes. Fortaleza's geographic coordinates are 322°E , 4°S . Its dip latitude is 2° . Cachoeira de Paulista's geographic coordinates are 315°E , 22.6°S , and its dip latitude is -26°S . Dr. M. A. Abdu of the Brazilian Institute for Space Research kindly has supplied plots of quantities derived from the ionosonde measurements made at these two stations on March 12 through 15, 1989. These quantities include $h_p\text{F2}$, the height of the F2 layer peak, and $h'\text{F2}$, the height of the base of the F2 region.

At Fortaleza, the base height of the F2 layer reached 750 km at 1900 LT (2130 UT) on March 13 and the apparent upward velocity of the F2 layer reached 230 m/s. The next time $h'\text{F2}$ could be determined at Fortaleza was 2030 LT (2300 UT) on March 13. At that time, it was about 650 km. At Cachoeira Paulista, $h'\text{F2}$ exceeded 770 km at 1900 LT (2200 UT) on March 13. At this time, the upward plasma velocity at Cachoeira Paulista was 136 m/s. The base height of the F2 layer was next determined at 2200 LT (0100 UT on March 14). These

data suggest that during the extremely large storm of March, 1989, the disturbance dynamo electric field elevated the equatorial F region above DMSP's 840 km altitude, producing the observed anomalously low densities in equatorial density. We recommend looking at total electron content and optical measurements from Cachoeira Paulista during this time period to see if they confirm this mechanism or indicate instead that chemical processes were largely responsible for the depletions.

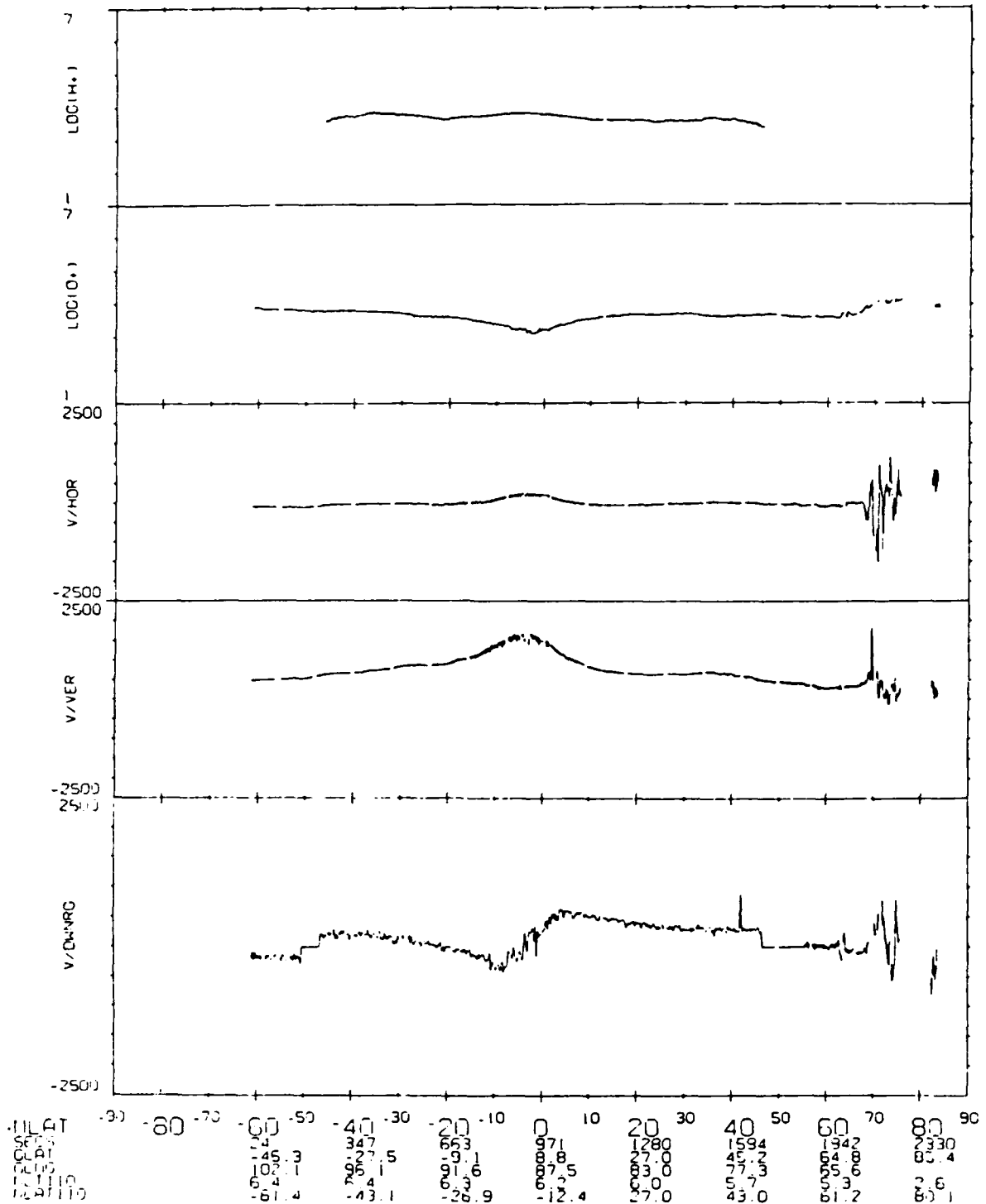


Figure 4-1 Three components of plasma drift and calculated O⁺ and H⁺ density as a function of sub-satellite magnetic latitude for an orbit on September 19, 1987. The drifts are in spacecraft coordinates. The bottom panel shows downrange drift, here positive southward. The second panel is vertical drift, with positive upward. The third panel is horizontal drift, here positive westward. Corotation has not been removed from the drifts. The scale is in m/s. The fourth and fifth panels show logs of the O⁺ and H⁺ concentrations in cm⁻³. The H⁺ concentration was calculated assuming that 85% of the light ions were H⁺ and 15% He⁺.

F 9 SSIES FRAME STARTS AT H/M = 0 / 24 SM ON M/D/Y = 3 / 14 / 1989

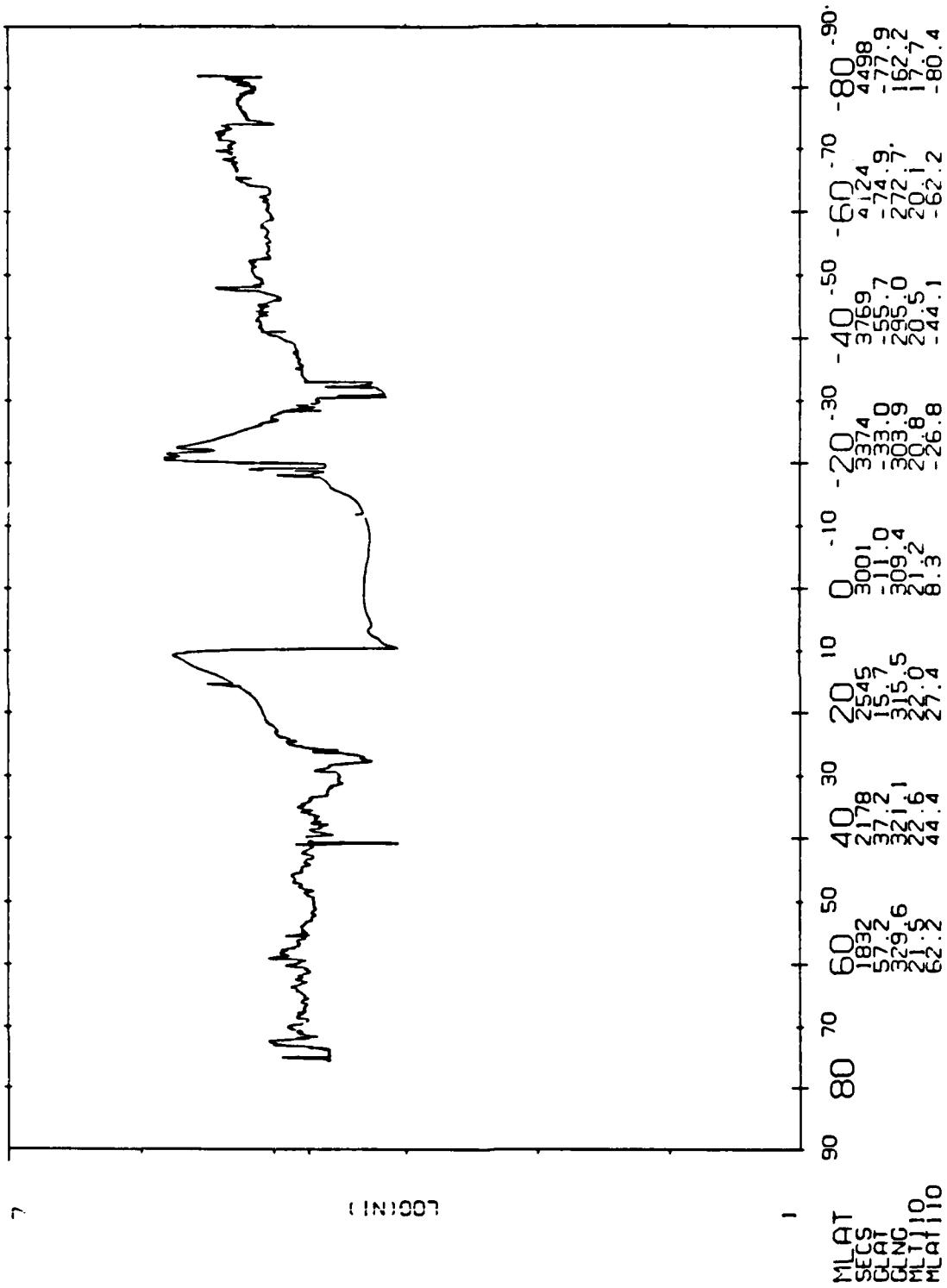


Figure 4-2 Log of total ion density in cm^{-3} measured by the DMSP F9 spacecraft between 0024 UT and 0114 UT on March 14, 1989 plotted as a function of magnetic latitude beneath the satellite.

F 9 SSIES FRAME STARTS AT H/M = 1 / 24 SM ON M/D/Y = 3 / 11 / 1989 FRM NO. 25

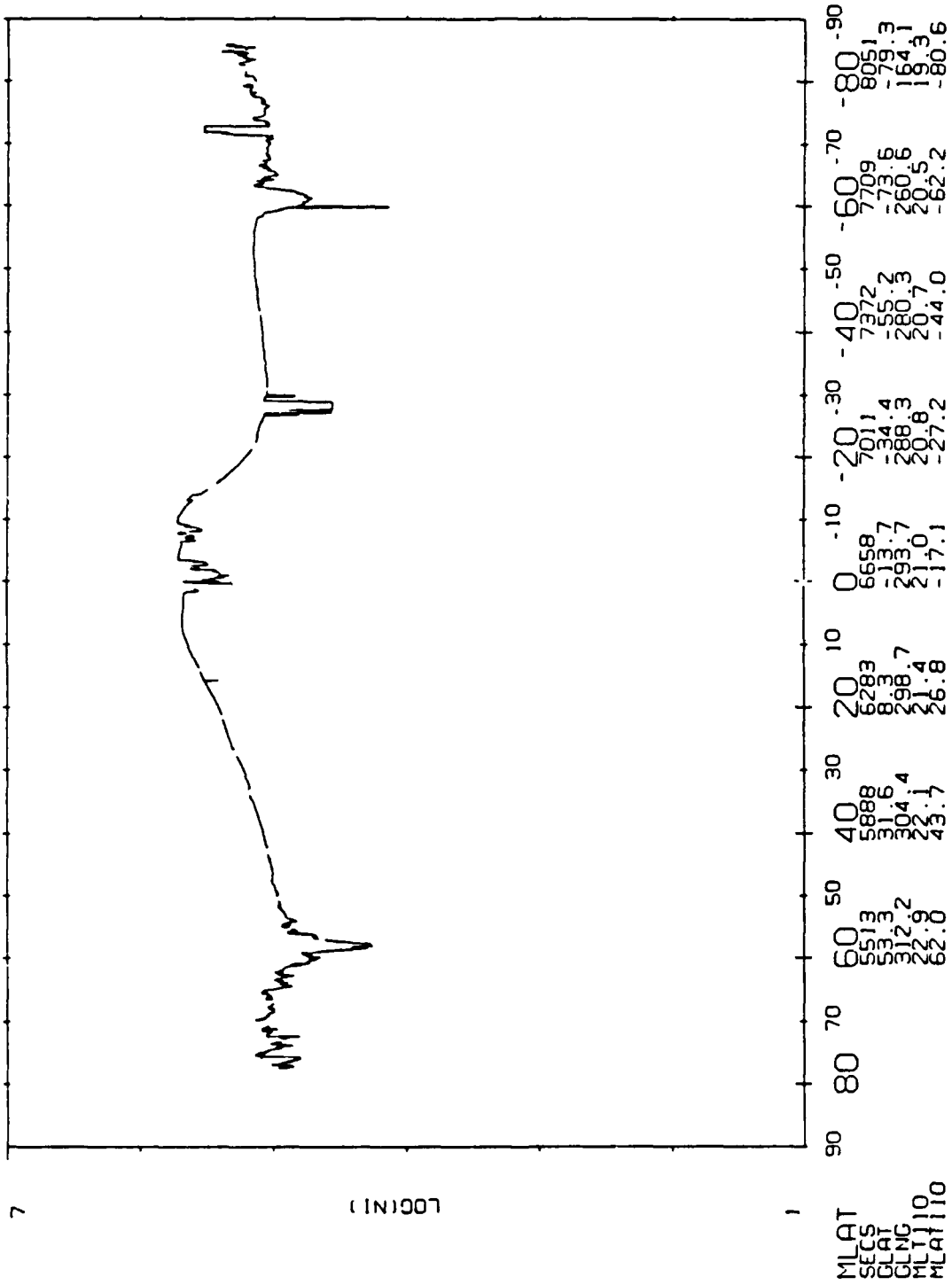


Figure 4-3 Log of total ion density in cm^{-3} measured by DMSP F9 between 0126 UT and 0216 UT on March 14, 1989 plotted as a function of magnetic latitude beneath the satellite.

5. DESIGN OF SPACE ENVIRONMENTAL SENSORS

5.1 Introduction

Regis College has provided engineering resources for the development of several GL (AFSC) Space Environmental Sensors. This work has included instrument design, evaluation, calibration and spacecraft integration. Overviews of the various instruments' purpose and function are presented in the following sections, along with descriptions of the specific activities performed by Regis College personnel in the development of each instrument.

5.2 DMSP: SSIES & SSIES-2

5.2.1 SSIES & SSIES-2 Overview

The purpose of the SSIES & SSIES-2 Plasma Monitor Systems is to obtain information about the characteristics of the space plasma (the electrically charged gas) above the peak (or maximum density region) of the F region of the ionosphere. This information is needed as input to ionospheric specification models required for efficient operational use of Air Force systems employing HF, VHF and UHF frequencies. The information will be obtained by four electrostatic probes to be flown on a series of satellites of the Defense Meteorological Satellite Program (DMSP).

The SSIES-2 system scheduled for launch on DMSP flights F11 - F15, is an upgraded design of the SSIES Plasma Monitor for flights F8 - F10. The major improvement is the added capability for in-flight block loading of the SSIES-2 main memory from the ground. This will significantly enhance in-flight operation by allowing real time adjustment to processing algorithms in reaction to unexpected measurement situations. Other changes include new and upgraded component selection and improved noise reduction by moving the sensitive electrometer amplifiers from the main electronics packages to their individual sensor

housings.

The major components of the SSIES-2 systems are: a) a microprocessor based Main Electronics Package (MEP), b) a Drift Scintillation Meter (DSM) Electronics Package, c) an Electron Electrometer Package, d) The Electron Sensor Assembly and e) an Ion Sensor Array Assembly as shown in Figure 5-1. The Ion Sensor Array Assembly consists of three cylindrical planar sensors, a triangular face plate (ground plane referenced to a bias) and a mounting bracket. This group of sensors includes the following: 1) Drift Meter Sensor, 2) Scintillation Meter Sensor and 3) Retarding Potential Analyzer (RPA). Each sensor is a cylinder with an aperture in the forward planar surface. An electrometer amplifier is mounted in the rear of each cylinder. The electron assembly consists of a boom mounted spherical electron sensor and an electron electrometer housing located near the base of the boom.

5.2.2.1 SSIES Activity

Engineering activities for the previously developed and delivered SSIES units on the DMSP S8, S9 and S10 spacecraft included review of integration test data, integration support and field services. Integration of the three spacecraft were processed in the following order: S9, S8 and S10. During the course of integrating each spacecraft, flight units were repeatedly tested by a ground based computer system. All downlinked telemetry data from the spacecraft was recorded on computer tape. For each of these tests GE Astro sent GL data from these computer tapes reproduced on stacks of printer paper. Engineering expertise was exercised in reviewing all of the above data. The S9 (F8) and S8 (F9) spacecraft have been launched from Vandenberg AFB and the S10 spacecraft has been placed in storage at Vandenberg ready for a future launch. Prior to shipping to Vandenberg, field service was

provided in support of a Preship Verification Tests at GE. Also, the SSIES system, installed on the S10 spacecraft, was modified as a result of the flight data received from F8 and F9 spacecraft. After several months of normal operation, serious anomalies were observed in the RPA and electron systems. After careful analysis of in-flight data, it was determined that the following modifications to the S10 instrument should be made. 1) To eliminate concerns of elevated in-flight temperatures with the RPA Sensor, the Lexan insulating material was replaced with Kel-F 81 which has a much higher temperature rating. 2) The electrometers were redesigned to provide better input protection from electrostatic discharges and a new high reliability input operational amplifier which had recently become available. 3) The flexprint backplane interconnection assembly in the Main Electronics Package was replaced with a new design as a result of failures experienced during integration of the SSIES-2 units. The new design eliminated stress on the flexprint solder joints that was causing cracking and poor electrical connection after long periods of time.

5.2.2.2 SSIES-2 Activity

The SSIES-2 systems are to be flown on spacecrafts S11, S12, S13, S14 and S15. The MEP, DSM electronics package, Drift Meter Sensor, Scintillation Meter Sensor and Ion Sensor Array Assembly were all developed under other GL contracts. This contract was responsible for the design and development of the electron and RPA electrometers and the analog circuitry in the MEP unit. Other direct involvement included all levels of systems engineering and related support activities.

Most of the design activity was completed on the previous contract, however, as a result of the design changes in the SSIES S10 instrument, it was necessary to incorporate the same electrometer circuit design changes into all of the SSIES-2 instruments. The new RPA Log

Electrometer circuit is shown in Figure 5-2 and the new Electron Log Electrometer circuit is shown in Figure 5-3.

System level activities included providing engineering expertise in developing the SSIES-2 instrument through delivery. All of the SSIES-2 instruments have been delivered to GE Astro Space Division. Before delivery, each system was integrated, environmentally tested, thermal cycled and calibrated. MEP units for S11, S12 and S13 had new PROM circuits and new flexprint interconnection assemblies installed after delivery. This activity corrected a bug in the flight software and stress problems experienced in the flexprint assemblies. After the MEP units were modified, they were requalified and redelivered. S11 and S12 have been fully integrated at GE Astro, S13 is presently going through integration and the other instruments are ready for integration.

5.3 CRRES

5.3.1 CRRES Overview

The purpose of the thirteen AFGL-701 instruments on the CRRES satellite is to determine the energetic particle fluxes throughout the earth's radiation belts and to determine the affect of energetic particles upon microelectronics. This goal will be achieved by a) measuring the particles' characteristics near the geomagnetic equator, b) measuring simultaneously the effects upon microelectronics, c) measuring those factors which cause changes in the energetic particle populations. Four of the thirteen instruments are combined to form a complement of experiments known as CRRES-225. These instruments are 1) AFGL-707-13-1, Fluxgate Magnetometer; 2) AFGL-701-13-2, Search Coil Magnetometer; 3) AFGL-701-14, Langmuir Probe; and 4) Passive Plasma Sounder. A block diagram of the above instruments is shown in Figure 5-4. GL has direct responsibility for the integration of all of these instruments.

5.3.1.1 AFGL-701-13-1 Overview

The purpose of the triaxial Fluxgate Magnetometer (AFGL-701-13-1) instrument is to obtain the ambient geomagnetic field and low frequency variations in that fields. This measurement will be used, 1) together with the look angles of the particle experiments to obtain pitch angles of the measured particles, 2) as a diagnostic of very low frequency waves in the ambient environment, and 4) to provide a secondary source of attitude information. The Fluxgate Magnetometer sensor is mounted on a rigid, 20 foot boom in order to get it far enough away from the spacecraft so that the total spacecraft generated magnetic field will be less than 2 nT. The electronics to operate the sensor is mounted inside the spacecraft with a link to the Langmuir Probe electronics which will provide power and telemetry. Each axis of the triaxial Fluxgate Magnetometer is sampled on two different ranges ($\pm 45,000$ nT and $\pm 1,000$ nT).

5.3.1.2 AFGL-701-13-2 Overview

The purpose of the Search Coil Magnetometer instrument is to obtain information on the plasma wave environment simultaneously with the Passive Plasma Sounder so that electric field fluctuations can be classified as due to electromagnetic or electrostatic waves and the plasma wave modes can be uniquely different. The Search Coil Magnetometer sensor is mounted on the same boom as the Fluxgate Magnetometer. The output from the sensor is fed through a 14 channel filter bank in the Passive Plasma Sounder instrument.

5.3.1.3 AFGL-701-14 Overview

The purpose of the Langmuir Probe instrument is to obtain the characteristics of the thermal plasma which can interact with the energetic particles through wave-particle interaction. This instrument is capable of both current collection for density determination

and voltage sensing for field measurements. The Langmuir Probe instrument consists of a pair spherical electron collectors mounted at the end of 50 meter wire booms. Each spherical collector contains a preamplifier and is connected to an electronics package for power, control and data processing. Interfaces are provided to two external cylinder wire boom preamplifiers and the Fluxgate Magnetometer. The electronics package supplies telemetry data to the spacecraft telemetry system and receives both serial and discrete commands from the spacecraft. Fluxgate Magnetometer digital data is made available on another external interface to the Low-Energy Plasma Analyzer (LEPA).

5.3.1.4 AFGL-701-15 Overview

The purpose of the Passive Plasma Sounder and Search Coil Magnetometer instruments, collectively known as the Plasma Wave experiment, is to measure the plasma wave environment in the earth's radiation belts and will also measure the electron number density. The Passive Plasma Sounder instrument consists of a 100 meter (tip to tip) cylinder wire boom (two 50 meter booms), two preamplifiers mounted near the base of the booms and an electronics package. The electronics package receives power and commands from the spacecraft. It provides interfaces with the spacecraft for the digitized data and an external interface with the Langmuir Probe for Search Coil analog data.

5.3.2.1 CRRES-225 Activity

System level engineering was provided for two integration periods during which the Fluxgate Magnetometer, the Search Coil Magnetometer, Langmuir Probe and the Passive Plasma Sounder instruments were integrated into a single system which entailed many responsibilities. Both integrations were completed at the facilities of the CRRES Prime Contractor, Ball Space System Division (BSSD). During the first integration the satellite was configured

for a shuttle launch. After program delays caused by the Challenger accident, the satellite was configured for an expendable launch vehicle (ELV). In between the two integration periods the instruments were returned to the experimenters for storage and calibration prior to redelivery. Other system responsibilities included maintaining system specifications and drawings and the CRRES-225 Interface Control Document (ICD). Documents for testing the CRRES-225 compliment of instruments during spacecraft integration tests were prepared. Prior to redelivering of the CRRES-225 instruments, the ICD Compliance Package was updated and delivered to Space Division. From this revised document, Space Division gave a certificate of approval to GL for redelivery of the instruments to BSSD.

Other activities included reintegrating the flight instruments at GL prior to redelivery. Other instrument activity included coordinating the reacceptance tests which included vibration, thermal/vacuum testing, burn-in and calibration.

5.3.2.2 AFGL-701-13-1 Activity

Engineering support was provide for the testing, calibration and integration of the Fluxgate Magnetometer manufactured by Schonstedt Instrument Company. Support was provided at NASA - GSFC in calibrating the instrument through the Langmuir Probe instrument. Other support included requalification testing with the Langmuir Probe instrument.

5.3.2.3 AFGL-701-14 Activity

The Langmuir Probe instrument consists of five units: 1) Electronics Package, AFGL-701-14A; 2) DC Preamplifier, AFGL-701-14B; 3) DC Preamplifier, AFGL-701-14C; 4) Wire Boom Assembly, AFGL-701-14D; and 5) Wire Boom Assembly, AFGL-701-14E. The preamplifiers were fabricated by NASA - GSFC and the wire booms were fabricated by Weitzmann Consulting. The AFGL-701-14A Electronics Package hardware was a responsibility of this

contract, including later modifications to the analog circuit designs which provided for a greater Fluxgate Magnetometer signal resolution. Another major modification was the installation of new PROM memory chips with upgraded flight software. Significant engineering support was provided during requalification testing and calibration at GL.

5.3.2.4 AFGL-701-15 Activity

The Passive Plasma Sounder instrument consists of five units as follows: 1) Electronics Package, AFGL-701-15A; 2) AC Preamplifier, AFGL-701-15B; 3) AC Preamplifier, AFGL-701-15C; 4) Wire Boom Assembly, AFGL-701-15D; and 5) Wire Boom Assembly, AFGL-701-15E. The electronics package and preamplifiers were fabricated by The University of Iowa. The boom assemblies were fabricated by Fairchild Space Company. Between the two integration periods, the boom assemblies went through EMI (ElectroMagnetic Interference) testing to determine the cause of an interference signal coupled into the wire boom output during spacecraft EMC/EMI testing. This interference signal was finally traced to the spacecraft EMC/EMI test setup which was verified during the second integration when the spacecraft was placed in an approved EMC/EMI chamber. Another activity developed during the requalification of the boom assemblies when one of the boom motors failed. Engineering support was provided to the manufacturer of the motor and Fairchild after it was discovered that the circuitry used in the brushless motors was prone to failures due to line transients. This problem was corrected prior to redelivery.

5.4 PASP

5.4.1 PASP Overview

The Photovoltaic Array Space Power (PASP) is a payload designed for shuttle missions. It is conceived to be as a series of integrated payloads to be carried on low-altitude, high

inclination space shuttle flights. Each payload mission will measure environmental interactions and their effect on candidate elements of planned Air Force space systems. As a part of the above payload, there will be a Langmuir Probe instrument for the measurement of electron density and electron temperature. The instrument hardware consists of an Electron Sensor and Main Electronics Package.

5.4.2 PASP Activity

Provided circuit design and system engineering expertise in the development of the Langmuir Probe instrument for the PASP payload. System design activity consisted of compiling the requirements of the GL scientists and the interface specifications from the Jet Propulsion Laboratory (JPL). The final system design consisted of an Electron Sensor, mounted on a boom provided by JPL, and a Main Electronics Package (MET). The Langmuir Probe measurement system is shown in Figure 5-5. Design of the MET started with a spare flight housing complete with an internal power supply from a previous program.

The MET in final form, as shown in Figure 5-6, consisted of the Power Supply, a Digital Board as shown in Figure 5-7, an Analog Board as shown in Figure 5-8 and a Translator Board.

System level activities included testing the flight boards and interfacing the Translator Board supplied by JPL. The instrument has been integrated with the PASP payload and will soon undergo environmental testing, calibration and be readied for flight.

5.5 IMPS

5.5.1 IMPS Overview

The Interactions Measurement Payload for Shuttle (IMPS), part of the GL Space Systems Environmental Interactions Technology Program, is conceived as a series of integrated

payloads to be carried on low-altitude, high-inclination space shuttle flights. Each IMPS mission will measure environmental interactions and their effect on candidate elements of planned Air Force space systems. As a part of the above payload, a Field and Plasma experiment was planned to investigate the shuttle/environment interactions and provide background data.

5.5.2 IMPS Activity

The IMPS Fields and Plasma program was canceled, however, prior to canceling support, was provided in the design of the input signal processing circuitry. The specifications provided for the input signal required that protection be included in the design to protect the preamplifier input circuitry from large transient voltages as result of spacecraft charging. The protection circuit selected was a miniature spark gap assembly which was mounted inside the wire boom mechanisms next to the output signal connector. Signals at the input of the preamplifier from the wire boom were anticipated to be between ± 90 volts. With these large signals, a preamplifier design using a high voltage operational amplifier was selected. The preamplifier schematic is shown in Figure 5-9. If power had been a consideration, a floating bias scheme would have been used such as was used in the CRRES preamplifiers.

5.6 POLAR

5.6.1 POLAR Overview

The POLAR Electric Fields Investigation (EFI) instrument is sponsored by NASA as a part of the International Solar-Terrestrial Physics (ISTP) program. The objective of the ISTP program is to study the origin of the solar variability and activity, the transport of manifestations of that activity to the earth via plasma processes, and the cause-and-effect relationships between that time varying energy transport and the near-earth environment.

The EFI instrument will be used to study the Global Geospace Science (GGS) to understand how the parts of this closely coupled, highly time-dependent system work together. The EFI instrument will be designed to study large parallel and perpendicular electric fields in double layers and electrostatic shocks; large spatial scale parallel electric fields responsible for upgoing ions and inverted-V electron acceleration; high latitude convection electric fields; and electric field structure of the high latitude magnetosphere, the polar cusp, and the plasma mantle.

5.6.2 POLAR Activity

The EFI instrument will be designed and developed for NASA by other contract organizations. Regis College was responsible for Participating in the design of the Ground Support Equipment (GSE) and preparation of Verification Plan document. The GSE will consist of an AT computer controlling a data acquisition unit and test equipment using the IEEE-488 interface. The data acquisition unit will have one special card designed to simulate the spacecraft interface and to control signals from the test equipment to the various flight components. The above GSE configuration is shown in Figure 5-10. The other major activity was writing a Verification Plan which will be used for environmental testing the flight unit at GL.

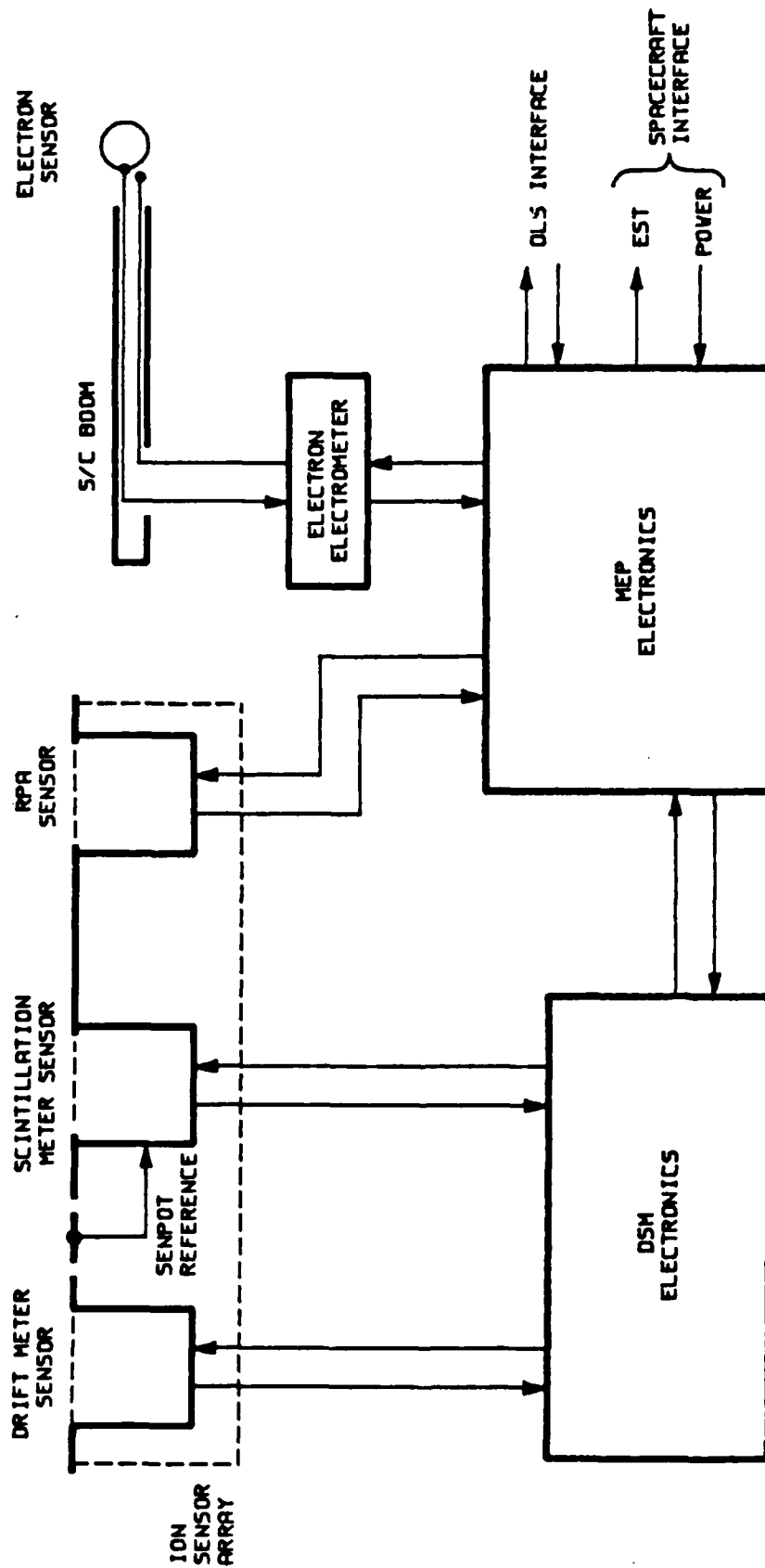


Figure 5-1 SSIJS-2 major components block diagram.

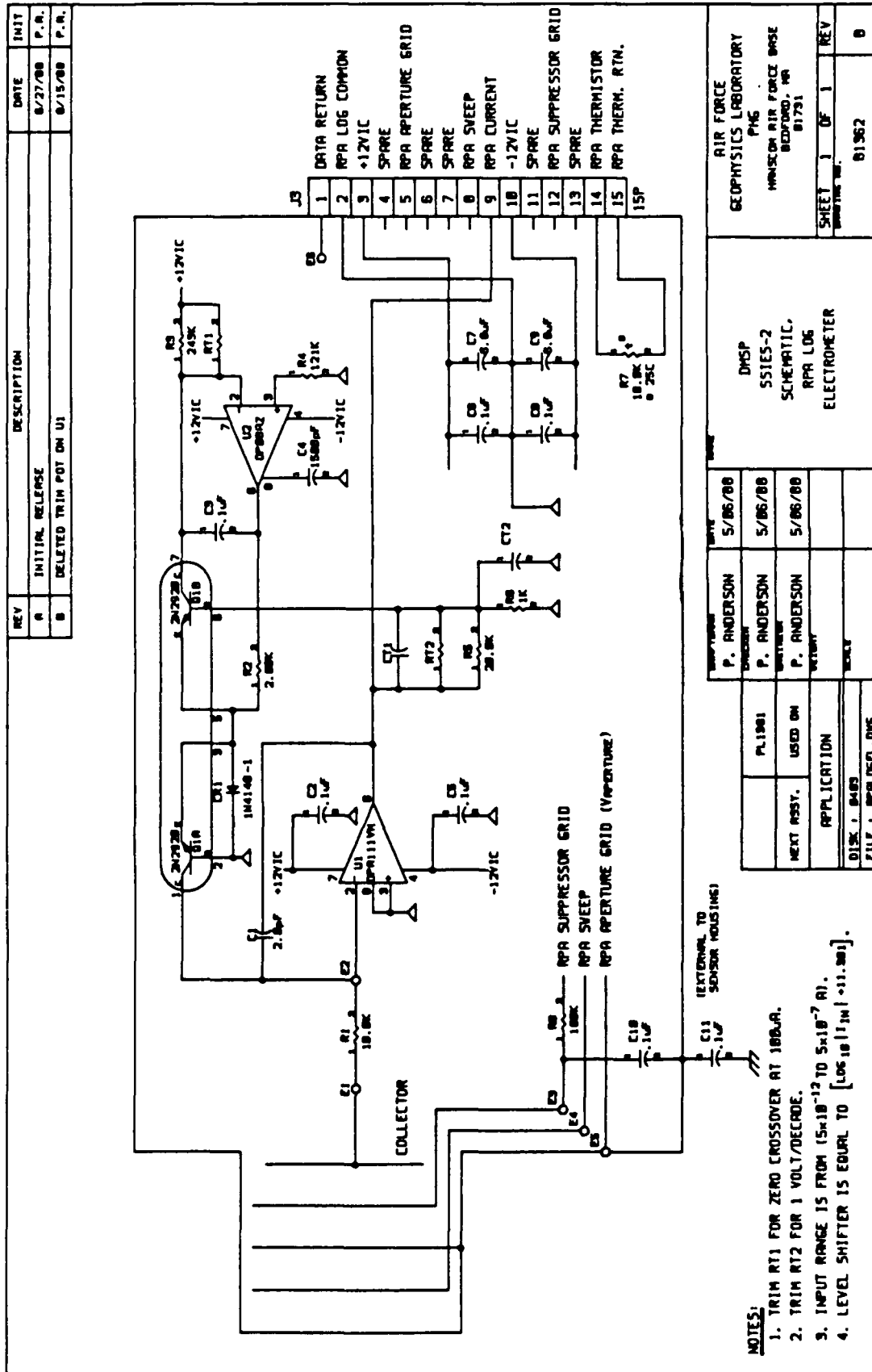
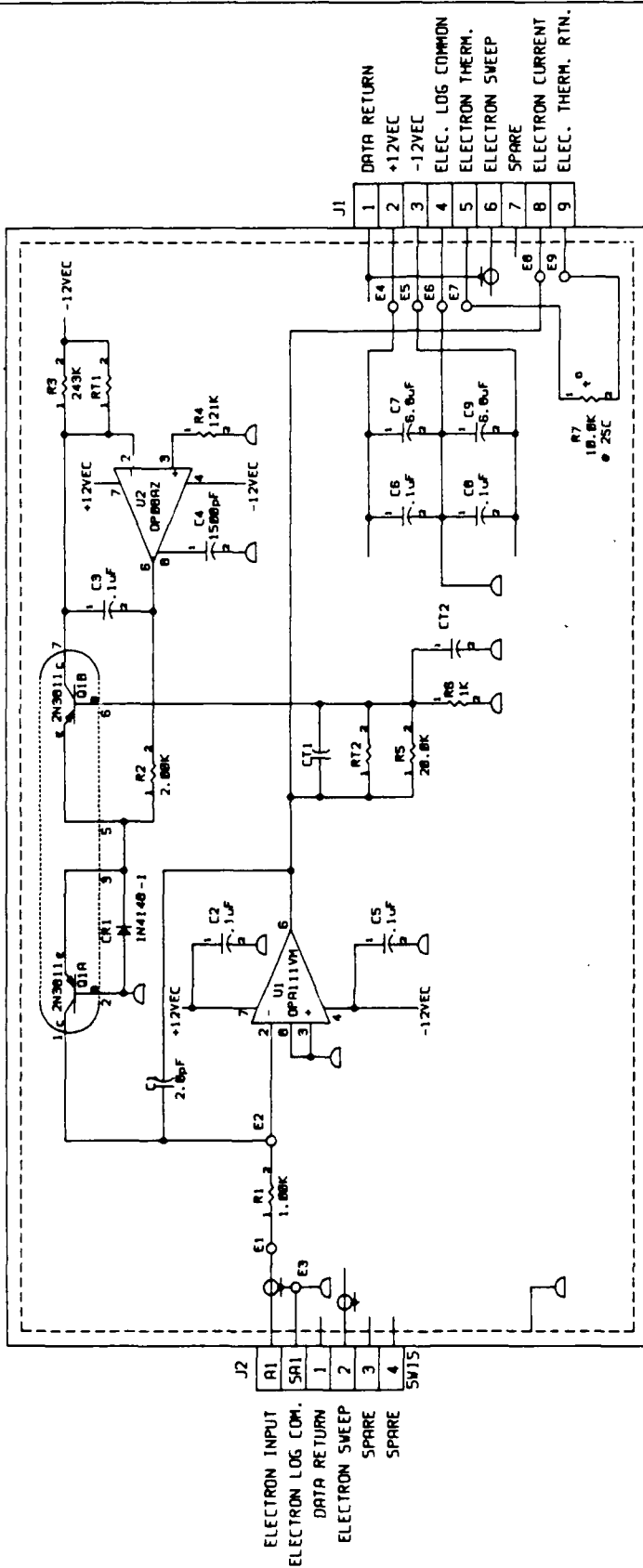


Figure 5-2 SSIES-2 schematic, new RPA log electrometer.

REV	DESCRIPTION	DATE	INIT
A	INITIAL RELEASE	6/27/88	P. A.
B	DELETED TRIM POT ON U1	8/15/88	P. A.



NOTES:

1. TRIM RT1 FOR ZERO CROSSOVER AT 100uA.
2. TRIM RT2 FOR 0.833 VOLTS/DECADE.
3. INPUT RANGE IS FROM $1 \cdot 10^{-10}$ TO -10^{-4} A.
4. EL SHIFTER OUTPUT IS EQUAL TO $5/6 [LOG_{10} |I_{IN}| + 10]$.

DESIGNER	DATE	MARK
P. ANDERSON	6/27/88	
PL 1363		
NEXT ASSY.	USED ON	
APPLICATION		
DISK 1 8483		
FILE 1 ELELOSEL.DWG		

DMSP	MARK
P. ANDERSON	6/27/88
DESIGNER	
WORKER	
VERIFY	
SCALE	

REV	DATE	BY	APPR
1	OF	1	REV
81364			B

AIR FORCE	GEOPHYSICS LABORATORY
PHG	DMSP
MANSCOM AIR FORCE BASE	SSIES-2
BEDFORD, MA	SCHEMATIC,
01731	ELECTRON LOG
	ELECTROMETER

Figure 5-3 SSIES-2 schematic, new electron log electrometer.

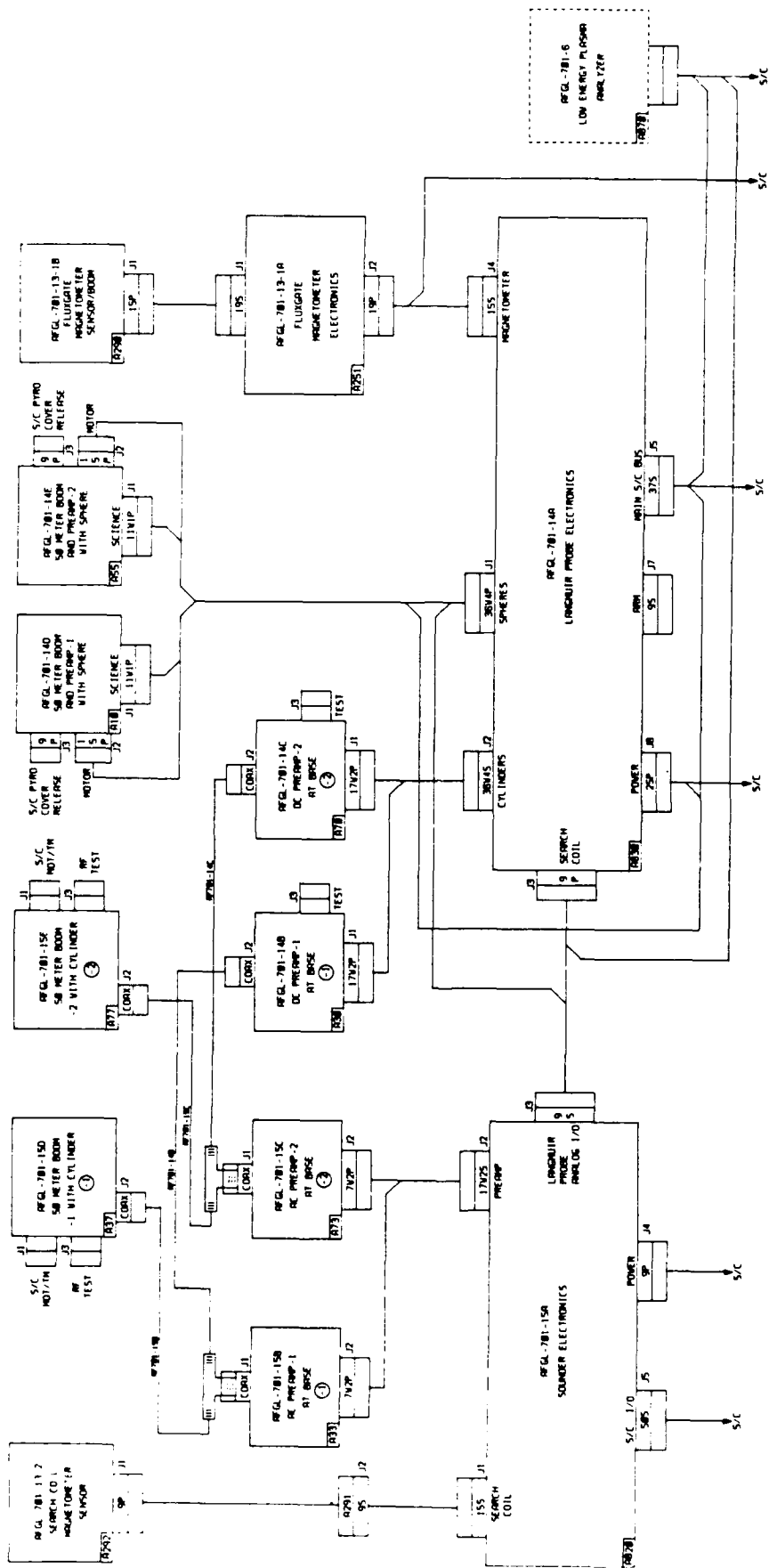


Figure 5-4 CRRES AFGL-701-13,-14,-15 interconnection block diagram.

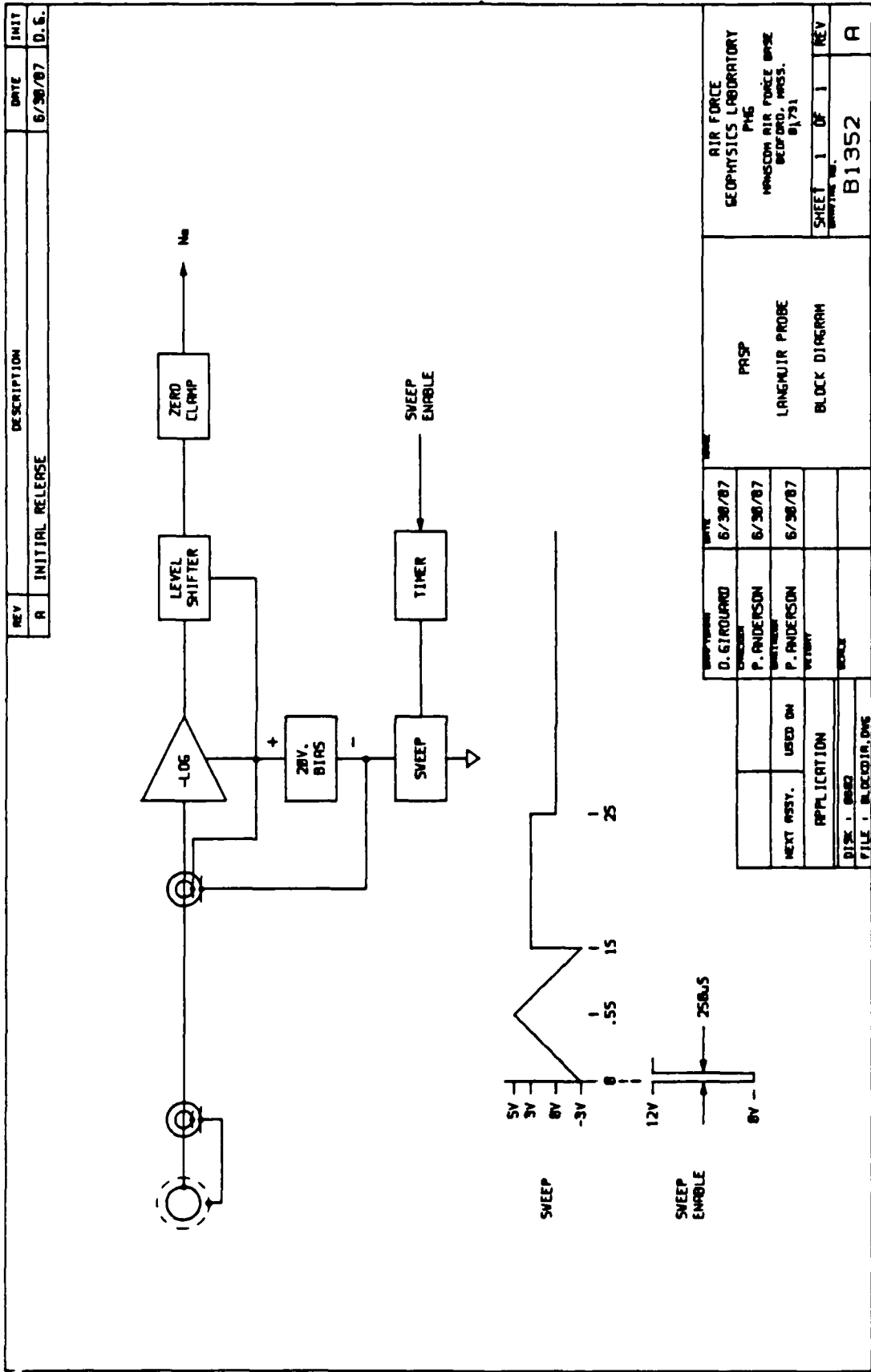
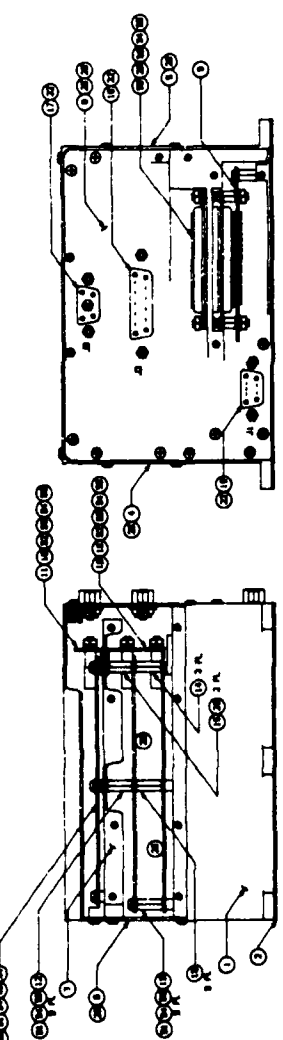
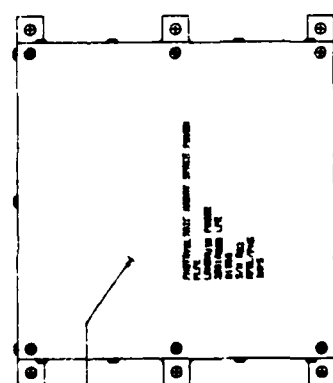


Figure 5-5 PASP Langmuir Probe block diagram.

17	17	37	127	1978-1	WIRE BOND BRUSH	
18	18	38	128	1978-1	WIRE BOND BRUSH	
19	19	39	129	1978-1	WIRE BOND BRUSH	
20	20	40	130	1978-1	WIRE BOND BRUSH	
21	21	41	131	1978-1	WIRE BOND BRUSH	
22	22	42	132	1978-1	WIRE BOND BRUSH	
23	23	43	133	1978-1	WIRE BOND BRUSH	
24	24	44	134	1978-1	WIRE BOND BRUSH	
25	25	45	135	1978-1	WIRE BOND BRUSH	
26	26	46	136	1978-1	WIRE BOND BRUSH	
27	27	47	137	1978-1	WIRE BOND BRUSH	
28	28	48	138	1978-1	WIRE BOND BRUSH	
29	29	49	139	1978-1	WIRE BOND BRUSH	
30	30	50	140	1978-1	WIRE BOND BRUSH	
31	31	51	141	1978-1	WIRE BOND BRUSH	
32	32	52	142	1978-1	WIRE BOND BRUSH	
33	33	53	143	1978-1	WIRE BOND BRUSH	
34	34	54	144	1978-1	WIRE BOND BRUSH	
35	35	55	145	1978-1	WIRE BOND BRUSH	
36	36	56	146	1978-1	WIRE BOND BRUSH	
37	37	57	147	1978-1	WIRE BOND BRUSH	
38	38	58	148	1978-1	WIRE BOND BRUSH	
39	39	59	149	1978-1	WIRE BOND BRUSH	
40	40	60	150	1978-1	WIRE BOND BRUSH	
41	41	61	151	1978-1	WIRE BOND BRUSH	
42	42	62	152	1978-1	WIRE BOND BRUSH	
43	43	63	153	1978-1	WIRE BOND BRUSH	
44	44	64	154	1978-1	WIRE BOND BRUSH	
45	45	65	155	1978-1	WIRE BOND BRUSH	
46	46	66	156	1978-1	WIRE BOND BRUSH	
47	47	67	157	1978-1	WIRE BOND BRUSH	
48	48	68	158	1978-1	WIRE BOND BRUSH	
49	49	69	159	1978-1	WIRE BOND BRUSH	
50	50	70	160	1978-1	WIRE BOND BRUSH	
51	51	71	161	1978-1	WIRE BOND BRUSH	
52	52	72	162	1978-1	WIRE BOND BRUSH	
53	53	73	163	1978-1	WIRE BOND BRUSH	
54	54	74	164	1978-1	WIRE BOND BRUSH	
55	55	75	165	1978-1	WIRE BOND BRUSH	
56	56	76	166	1978-1	WIRE BOND BRUSH	
57	57	77	167	1978-1	WIRE BOND BRUSH	
58	58	78	168	1978-1	WIRE BOND BRUSH	
59	59	79	169	1978-1	WIRE BOND BRUSH	
60	60	80	170	1978-1	WIRE BOND BRUSH	
61	61	81	171	1978-1	WIRE BOND BRUSH	
62	62	82	172	1978-1	WIRE BOND BRUSH	
63	63	83	173	1978-1	WIRE BOND BRUSH	
64	64	84	174	1978-1	WIRE BOND BRUSH	
65	65	85	175	1978-1	WIRE BOND BRUSH	
66	66	86	176	1978-1	WIRE BOND BRUSH	
67	67	87	177	1978-1	WIRE BOND BRUSH	
68	68	88	178	1978-1	WIRE BOND BRUSH	
69	69	89	179	1978-1	WIRE BOND BRUSH	
70	70	90	180	1978-1	WIRE BOND BRUSH	
71	71	91	181	1978-1	WIRE BOND BRUSH	
72	72	92	182	1978-1	WIRE BOND BRUSH	
73	73	93	183	1978-1	WIRE BOND BRUSH	
74	74	94	184	1978-1	WIRE BOND BRUSH	
75	75	95	185	1978-1	WIRE BOND BRUSH	
76	76	96	186	1978-1	WIRE BOND BRUSH	
77	77	97	187	1978-1	WIRE BOND BRUSH	
78	78	98	188	1978-1	WIRE BOND BRUSH	
79	79	99	189	1978-1	WIRE BOND BRUSH	
80	80	100	190	1978-1	WIRE BOND BRUSH	
81	81	101	191	1978-1	WIRE BOND BRUSH	
82	82	102	192	1978-1	WIRE BOND BRUSH	
83	83	103	193	1978-1	WIRE BOND BRUSH	
84	84	104	194	1978-1	WIRE BOND BRUSH	
85	85	105	195	1978-1	WIRE BOND BRUSH	
86	86	106	196	1978-1	WIRE BOND BRUSH	
87	87	107	197	1978-1	WIRE BOND BRUSH	
88	88	108	198	1978-1	WIRE BOND BRUSH	
89	89	109	199	1978-1	WIRE BOND BRUSH	
90	90	110	200	1978-1	WIRE BOND BRUSH	



SIDE VIEW - SIDE COVER REMOVED

DATE	BY	APPROVED	REV	013558
				R
PARTS LIST				
PASP				
LITHIUM POWER				
REPEATER UNIT				
SERIAL 1000000				
REV. 013558				

Figure 5-6 PASP assembly diagram, main electronics package.

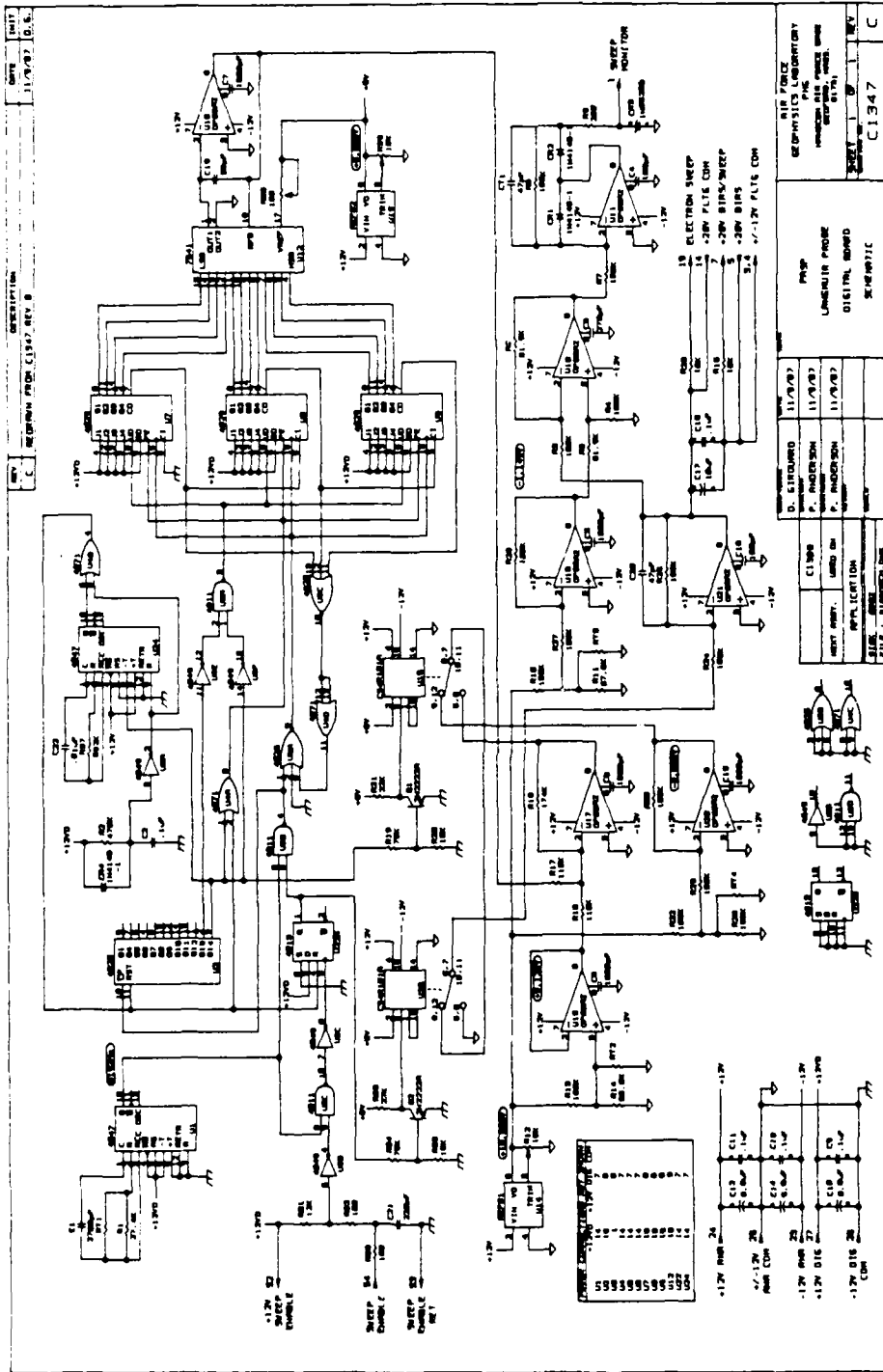


Figure 5-7 PASP schematic, digital electronics.

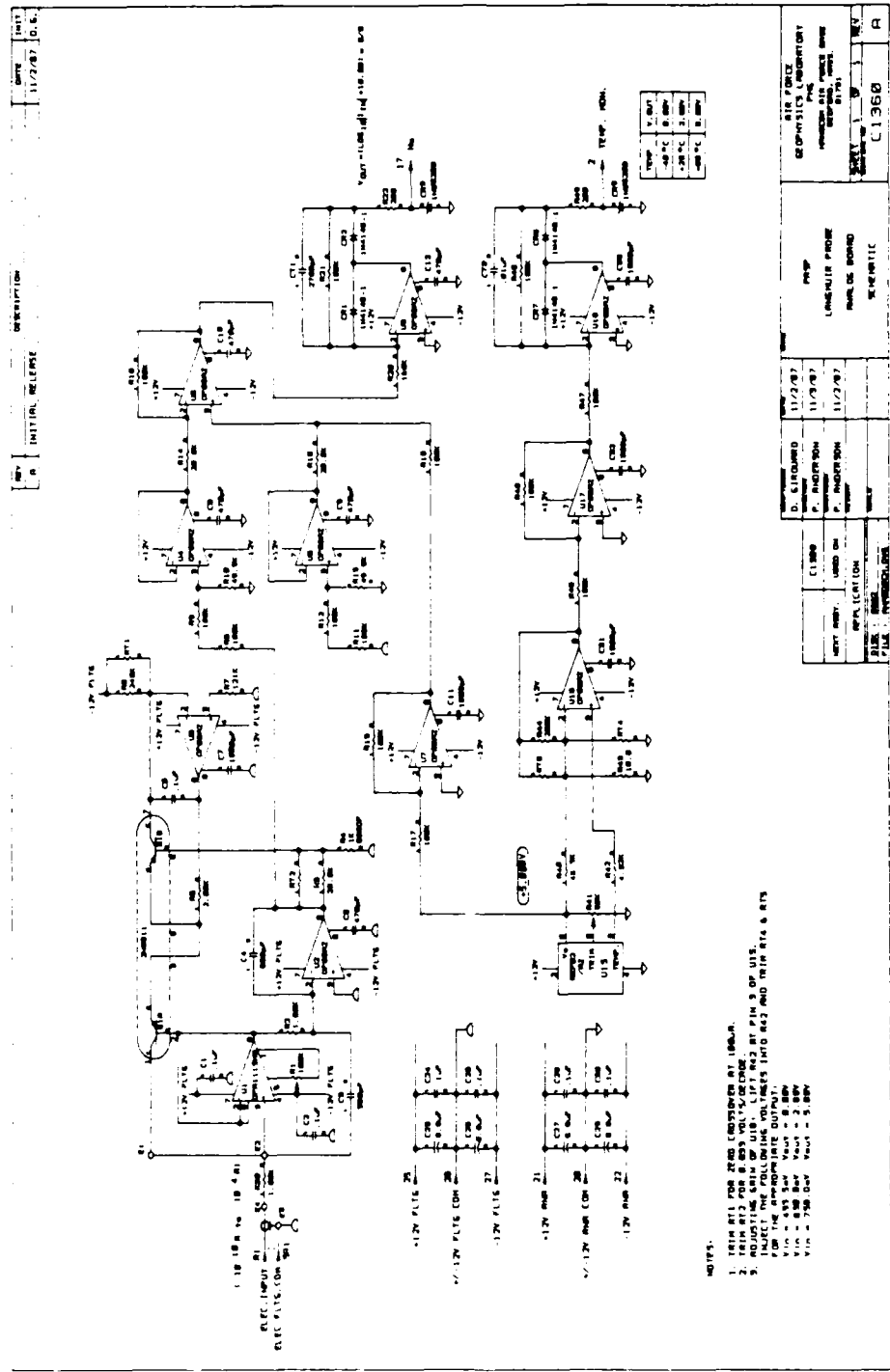
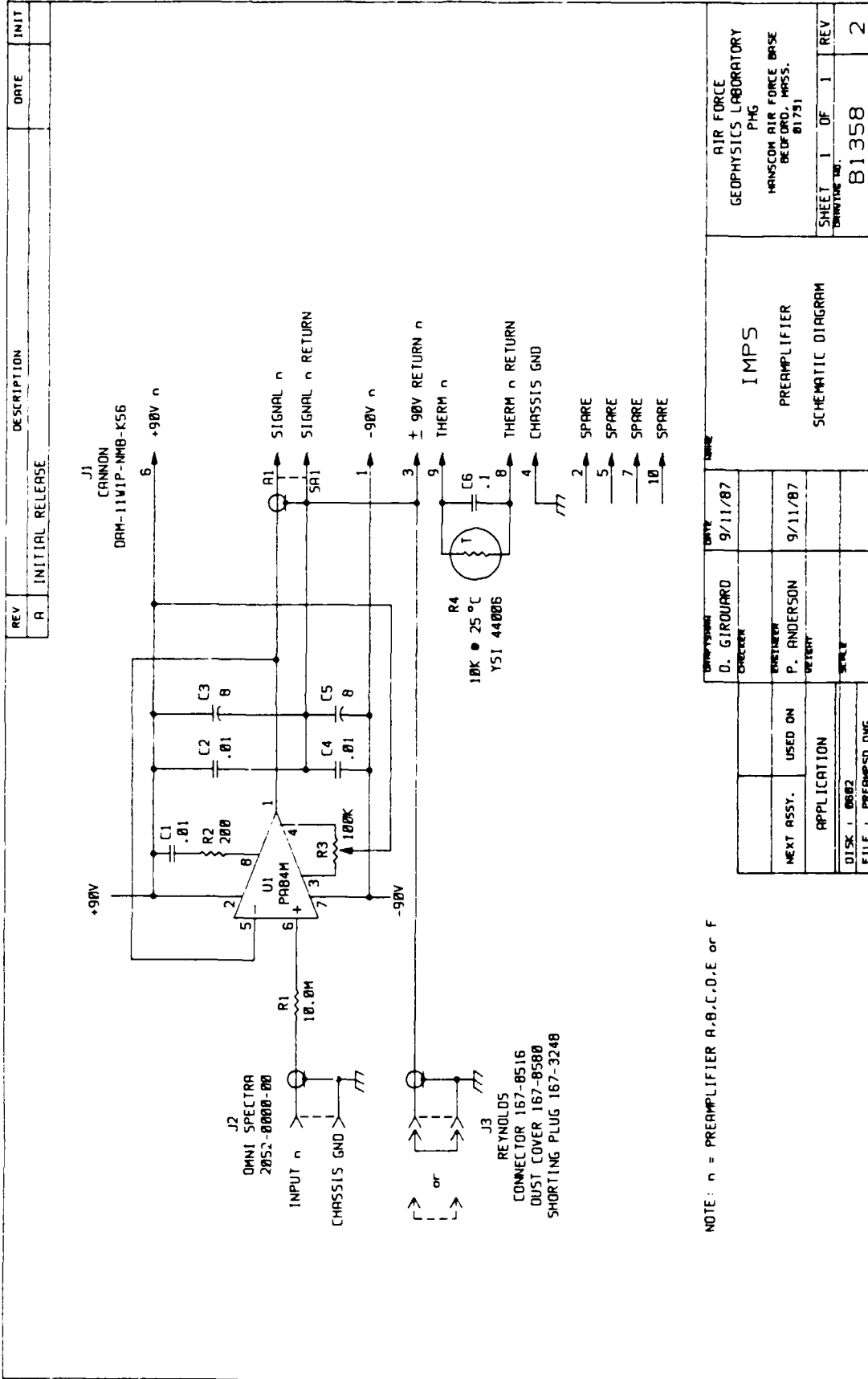


Figure 5-8 PASP schematic, analog electronics.



DESIGNER D. GIRAUD CHECKER	DATE 9/11/87	DRAWN P. ANDERSON CHECKED W. BERRY	DATE 9/11/87	SCALE 1:1
NEXT ASSY. USED ON		APPLICATION		
DISK 1 0002		FILE 1 PREAMP5D.DWG		
IMPS PREAMPLIFIER SCHEMATIC DIAGRAM		AIR FORCE GEOPHYSICS LABORATORY PHG HANSCOM AIR FORCE BASE BEDFORD, MASS. 01731		
SHEET 1 OF 1		REV 1		REV 2
DRAWING NO.		81358		

Figure 5-9 IMPS schematic, preamplifier electronics.

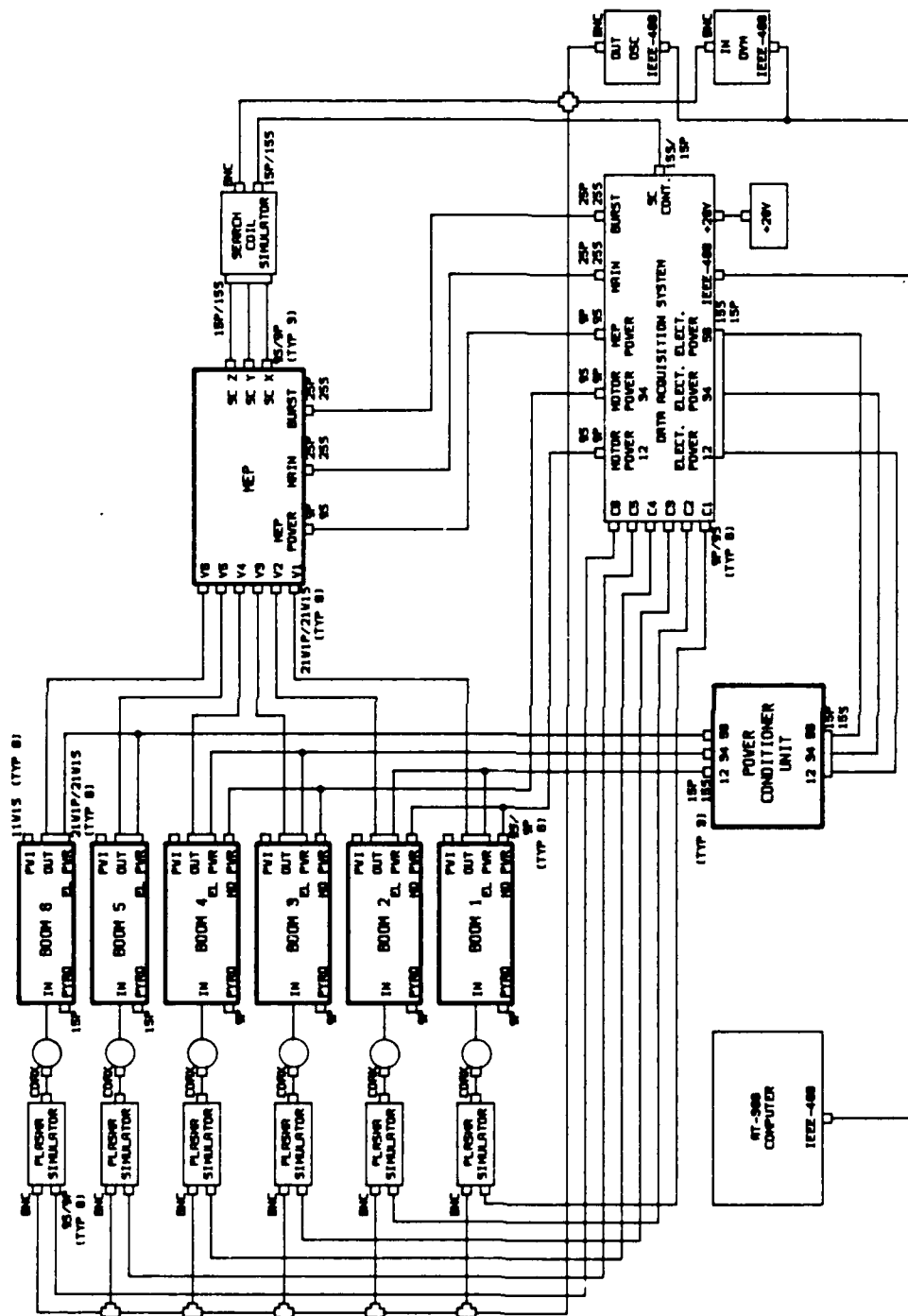


Figure 5-10 POLAR Electric Field Instrument block diagram with GSE.

6. DATA PROCESSING AND ANALYSIS

6.1 SSIES Data Processing

The Phase I stage of SSIES data reduction was developed by Boston College who also maintains and executes the software. Regis College obtained knowledge of their tape data base through files called F8IESDB and F9IESDB under username = RDMSPP which are public domain. Boston College was responsible for putting Phase II in its final version which is the production model now in use. However, Regis College is now responsible for the maintenance of the code and rewriting any problem areas. Phase II for F8 from Nov 87 through Jan 90 and for F9 from Feb 88 through Dec 89 has been processed. The record keeping for these production runs is maintained under these two filenames, F8IESDB under username James and F9IESDB under username Regis. The files are public domain which is how other users have access to the data.

Regis College developed the Phase III software for the final stage of the SSIES data reduction. For the F8 data from periods Nov 87 through June 88 and the F9 data from period Feb 88 through Sep 88, two complete sets of fiche were completed. They were sent to University of Texas at Dallas per their request. At this time, the practice of making double fiche has been abandoned and we are now processing every 5th day of the month to obtain a survey. Processing of the data has been completed up to May 89 for F9 and up to Oct 89 for F8.

The Phase III executable binary has been incorporated into a procedure which makes the job set-up extremely easy. One can choose batch or interactive processing along with a whole host of other options. The program has been modified to plot by degree as well as the original way-by time. Within the heading of degree, one can select polar plots which follow

the GMLAT from 0,90,0 or one can select equatorial plots which follow the GMLAT from 90,0,-90 and around the other side of the earth. There are also choices available for you to change the ranges and rearrange the plotting sections within an instrument.

Figures 6-1, 6-2 and 6-3 show FS data from Oct 22, 1987 in the south pole which shows the development of Phase III and the various ways for displaying the same data. These plots are in demand and have been requested by the following scientists: Sunanda Basu of Boston College, Dwight Decker of Boston College, Geoff Crowley of University of Lowell, Paul Cannon of University of Lowell and Huey-Ching Yeh of Millstone Hill Observatory.

6.2 RPA Sweep Analysis Program

A new computer program was developed by Regis College personnel in order to process the data from the Retarding Potential Analyzer (RPA) on the SSIES instrument. This instrument basically consists of a collector plate which draws current from the ions in the ambient plasma around the DMSP satellite. The current is a function of the voltage applied to a grid over the collector plate. In order to obtain one measurement, the current is measured as the voltage is varied from -2.91 volts to +11.91 volts during a period of 4 seconds. The result is a current-voltage curve which may look like the example shown in Figure 6-4. A FORTRAN subroutine was written in order to derive from this I-V curve the ion temperature, the ion drift velocity, and the densities of the hydrogen, helium, and oxygen ions. At times there may be only one or two ion species present, or there may be "bad" data, so the subroutine had to be "smart" enough to handle a variety of situations.

The logic of the program is based upon the following equation for the current as a

function of voltage:

$$I = \frac{AqV}{2} \sum_{i=1}^n \left\{ N_i \left[1 + \operatorname{erf}(x_i) + \frac{a_i \exp(-x_i^2)}{V\sqrt{\pi}} \right] \right\} \quad (6a)$$

$$x_i = \frac{V}{a_i} - \sqrt{\frac{q\phi}{kT}} \quad \text{for } \phi \geq 0$$

$$x_i = \frac{V}{a_i} \quad \text{for } \phi < 0 \quad (6b)$$

$$a_i = \sqrt{\frac{2kT}{m_i}} \quad (6c)$$

$$V = V_{sat} + V_{drift} \quad (6d)$$

$$\phi = \phi_{ap} + \phi_{sweep} \quad (6e)$$

In this equation, I is the collector current, V_{sat} is the velocity of the satellite, V_{drift} is the ion drift velocity, ϕ_{ap} is the instrument aperture potential, ϕ_{sweep} is the sweep potential or voltage applied to the grid, A is the sensor collector area multiplied by a grid transparency factor, q is the electron charge, n is the number of ion species, m_i is the mass of species i , N_i is the number density of species i , k is Boltzman's constant, and T is the temperature. The term on the far right side of Equation 6a is usually very small and can be assumed to be nearly zero.

The logarithm of Equation 6a, with the small term dropped, is:

$$\log I + \log \left(\frac{Aq}{2} \right) + \log V + \log \left\{ \sum_{i=1}^n N_i [1 + \operatorname{erf}(x_i)] \right\} \quad (7)$$

At the low-voltage end of the I-V curve the heavy-ion (assumed to be oxygen) current is constant, and at the high-voltage end of the curve the light-ion (assumed to be hydrogen) current is zero. Therefore, in certain regions of the curve the current is affected only by heavy or light ions. For just one ion species present, Equation 7 takes on the form:

$$\log I = \log \left(\frac{Aq}{2} \right) + \log V + \log N_i + \log [1 + \operatorname{erf}(x_i)] \quad (8)$$

At the voltage where $x_i = 0$ the current is one-half of its low-voltage saturation level, and the base 10 logarithm is down by $\log_{10} 2$. At this same voltage the derivative of $\log_{10} I$ has the value

$$\left. \frac{\partial \log I}{\partial \phi} \right|_{x_i=0} = - \left(\frac{q}{\pi k T \phi} \right)^{1/2} \quad (9)$$

where

$$\phi|_{x_i=0} = \phi_{ap} + \phi_{sweep} = \frac{m_i V^2}{2q} \quad (10)$$

Therefore, the ion temperature can be determined from the derivative at the one-half point, if the aperture potential is known or the ion velocity is known.

With these basic principals in mind, the RPA sweep analysis subroutine proceeds in the following manner. First the program needs to determine if both light and heavy ions are present, on the basis of the ratio of the currents at low and intermediate voltages. If both types are present then the heavy-ion saturation current is found (I_o in Figure 6-4). The code next locates the voltage ϕ_o , where the current is one-half of I_o , and the derivative of $\log_{10} I$ at that voltage. The constant I_o is subtracted from the entire curve before proceeding to find the light-ion saturation current, I_H , and the voltage ϕ_H . From Equation 6b and the condition that $x_i = 0$ at the one-half points, it is known that

$$m_o V^2 = 2q(\phi_o + \phi_{ap}) \quad (11)$$

and

$$m_H V^2 = 2q(\phi_H + \phi_{ap}) \quad (12)$$

These two simultaneous equations are solved to find the velocity and the aperture potential

$$V = \left[\frac{2q(\phi_o - \phi_H)}{m_o m_H} \right]^{1/2} \quad (13)$$

$$\phi_{ap} = \frac{m_O V^2}{2q} - \phi_O \quad (14)$$

which can then be used to calculate the ion temperature, using Equation 9. The subroutine can then use these derived values for the velocity, aperture potential, and temperature (which were derived with the assumption that all of the light-ion current is due to hydrogen, and there is very little helium present) in order to calculate the hydrogen and oxygen number densities, using the saturation currents I_O and I_H and Equation 8. As an option, the subroutine can use these values as a first estimate which is then used by a non-linear, Simplex method curve-fitting routine (which uses more computer time). This routine fits Equation 6a to the measured I-V curve, using three ion species, in order to find both the helium and hydrogen densities. The signal due to the helium is not easy to distinguish from the hydrogen since their masses and cut-off voltages are so close together.

If in the initial stage of the subroutine it determines that only light or heavy ions are present, then the program works along much the same lines as with two species, but in order to determine the temperature it is necessary to assume that the drift velocity is zero (and the velocity is the satellite velocity) if the latitude is low, or else use the last known value for the aperture potential. In summary, this RPA sweep analysis subroutine has been found to be faster and more accurate than previous programs, and it has been incorporated into the routine processing of the SSIES RPA data.

6.3 Removal of Corotation from SSIES Drift Data

Leonid Pereplyotchik was employed by Regis College as a temporary programmer from mid-October to mid-December, 1989. During this period, he wrote a program to combine SSIES RPA and drift meter velocity measurements, subtract corotation, put the model magnetic field into spacecraft coordinates, and plot the results. Because the SSIES RPA

•
-
-
can measure the downrange drift once every four seconds while the drift meter makes six measurements of the two perpendicular velocity components each second, the drift meter measurements taken during one four-second RPA sweep are averaged. Then the corotation velocity is calculated in earth-centered inertial coordinates. It is transformed into spacecraft coordinates and the appropriate components are subtracted from the downrange and horizontal drift velocities. Finally, the model magnetic field is transformed from geographic to spacecraft coordinates and interpolated so that vector magnetic field values are available once every four seconds in synchrony with the drift measurements. The program is designed to handle periods when either the RPA or the drift meter data are missing. This program will be used to determine the components of the plasma flow parallel and perpendicular to the earth's magnetic field and as a basis for making clock plots of the SSIES ion drift velocities.

6.4 Digitizing Models of Plasma Convection

Empirical models of the high-latitude plasma convection/electric potential had been published by Heppner and Maynard²⁶. The published form of these models consisted of contour plots of the average electric potential for different orientations of the interplanetary magnetic field. It had been necessary to convert these empirical models from drafted illustrations into a digital form. In order to develop these models further, compare them to other models, or use them in numerical calculations. Regis College personnel working on this contract traced the Heppner-Maynard patterns with a digitizing device, then developed software to convert the tracings to digital representations having uniformly spaced grid points. GL scientists subsequently used these digital data to develop functional representations of

²⁶ Heppner, J. P., and N. C. Maynard, Empirical high-latitude electric field models, *J. Geophys. Res.*, 92, 4467, 1987

the electrostatic potential patterns. Rich and Maynard have published the results of this research²⁷.

²⁷ Rich, F. J., and N. C. Maynard, Consequences of using simple analytical functions for the high-latitude convection electric field, *J. Geophys. Res.*, 94, 3687, 1989

F 8 SSIES FRAME STARTS AT H/M = 1 / 7 DM ON M/D/Y = 10/ 22 / 1987 FRM NO. 3

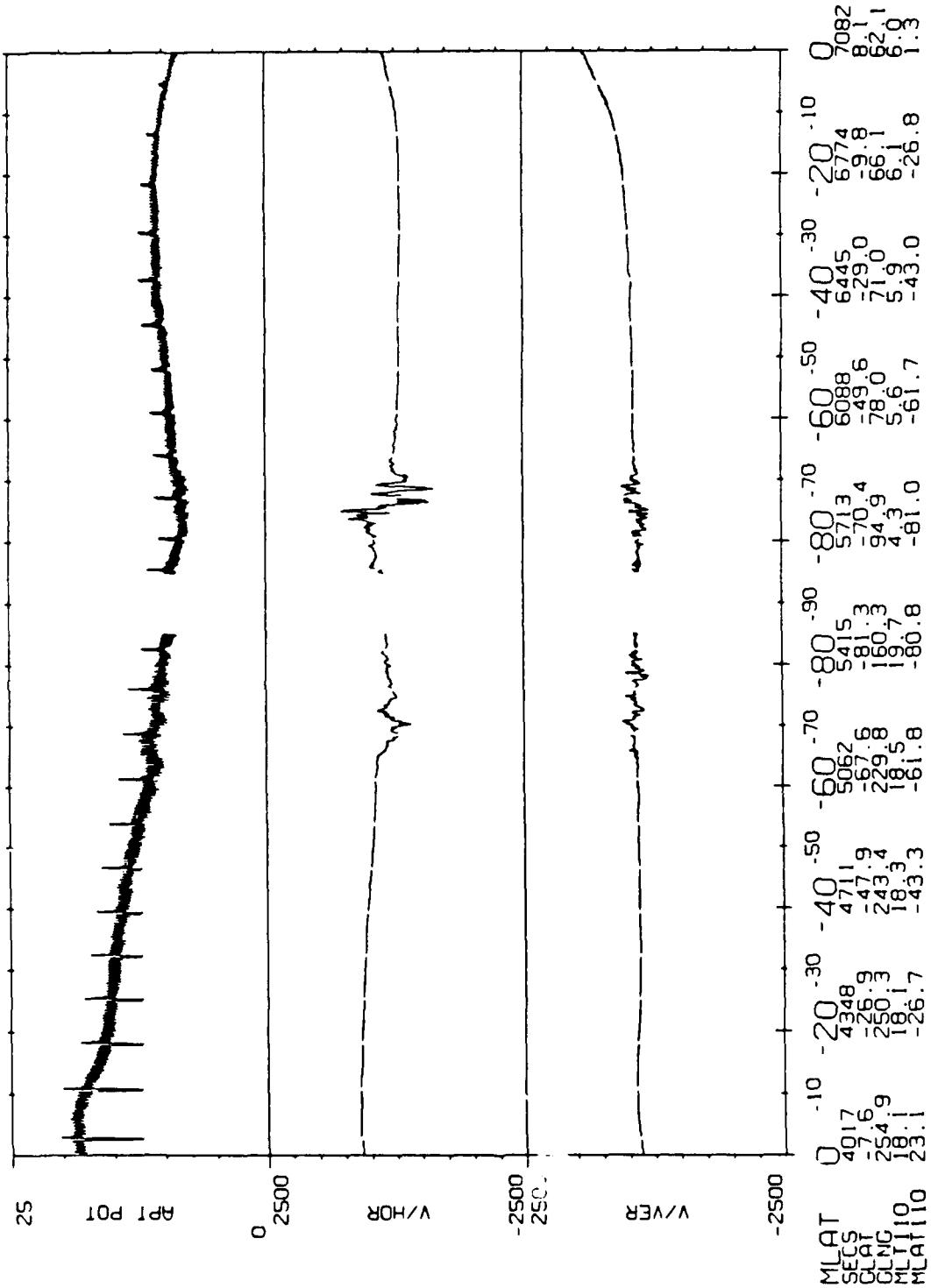


Figure 6-1 A pass of 52 minutes. The x-axis is time in seconds.

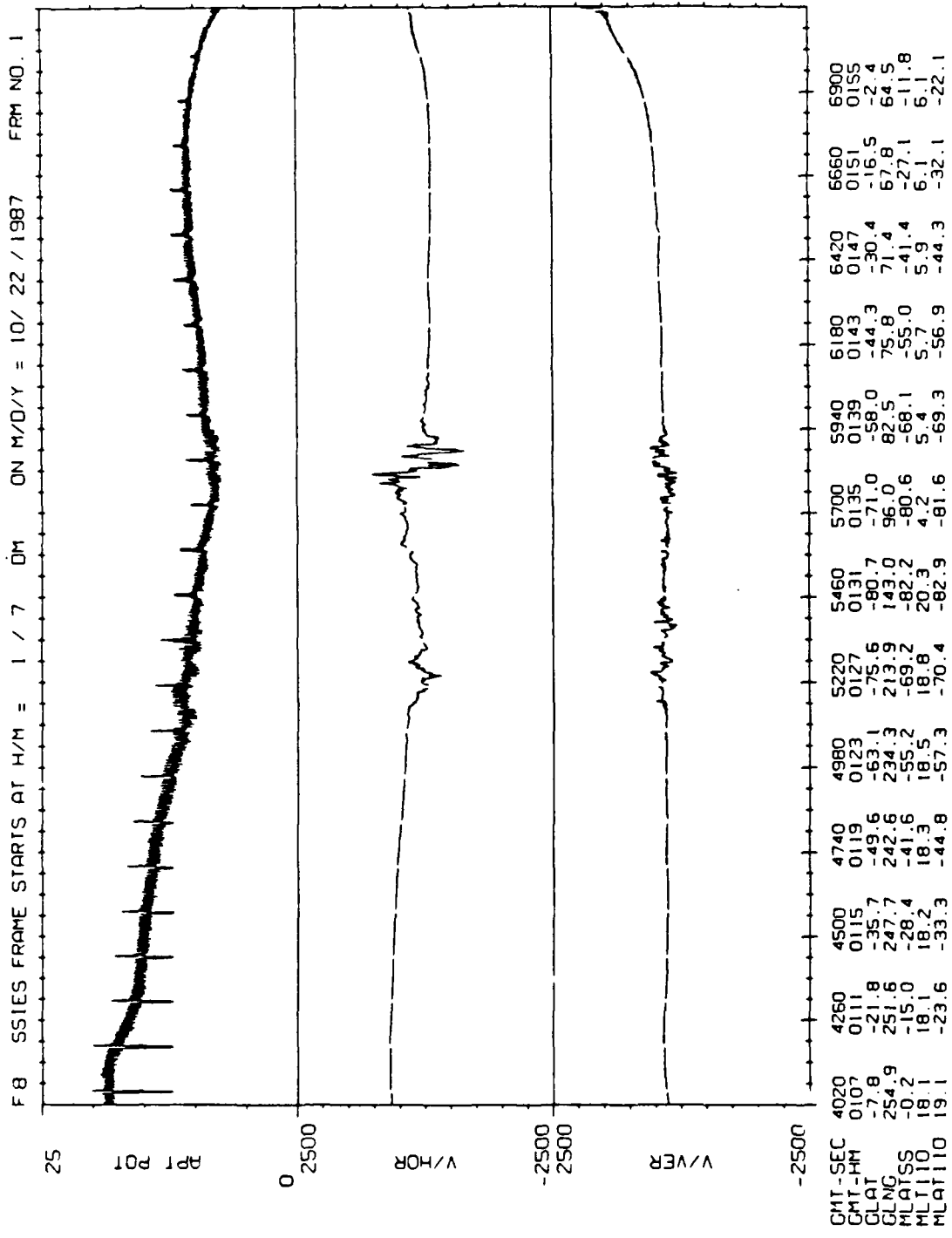


Figure 6-2 The same pass plotted with the options of degree and polar. The x-axis is gmlat-sub satellite.

F 8 SSIES FRAME STARTS AT H/M = 1 / 7 0M ON M/D/Y = 10/ 22 / 1987 FRM NO. 1

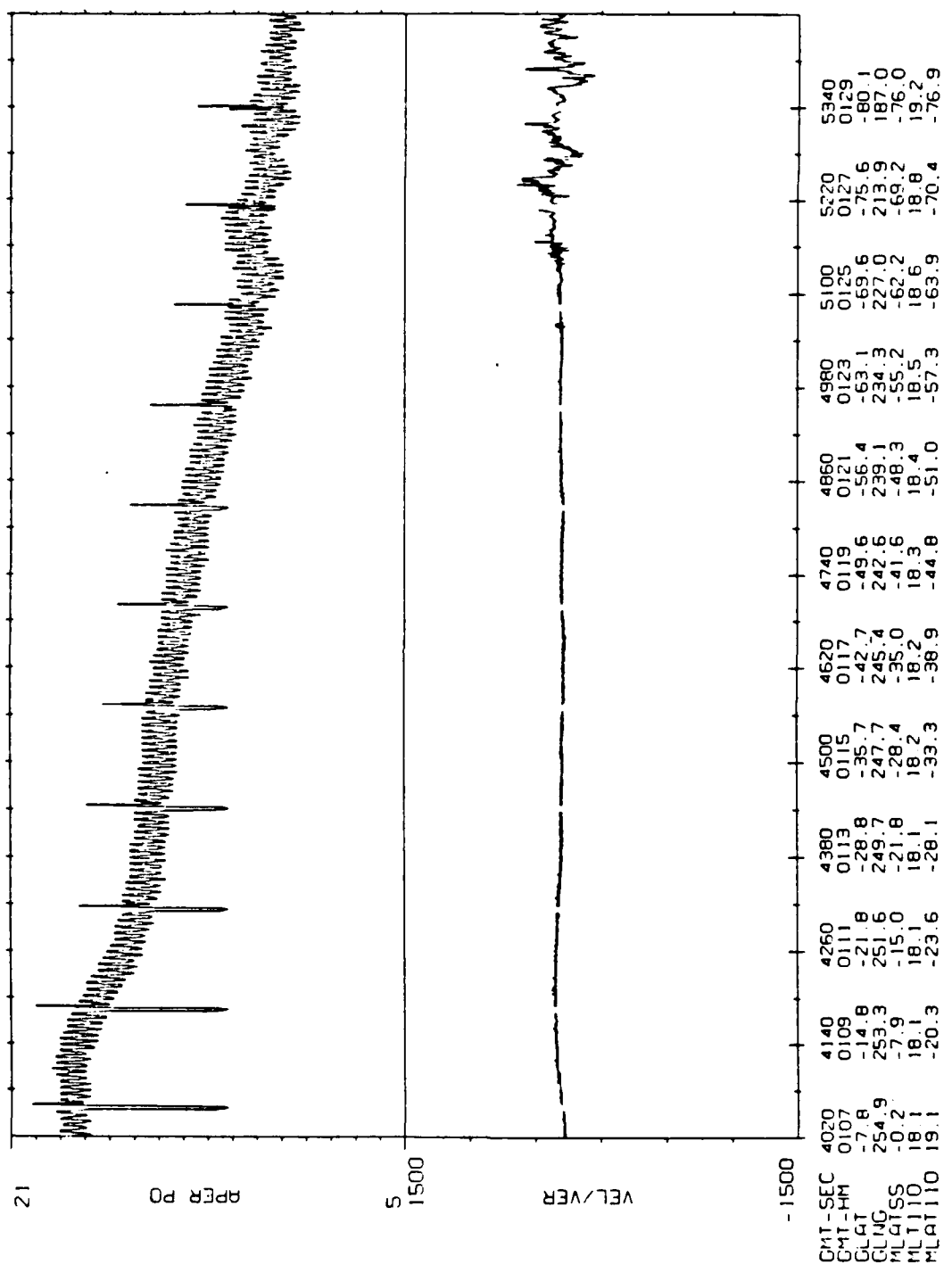


Figure 6-3 Twenty-four minutes of a time plot starting at 1:07 as the others. However, this time we eliminated v/hor and changed the ranges of the other two measurements.

SSIES RPA SWEEP

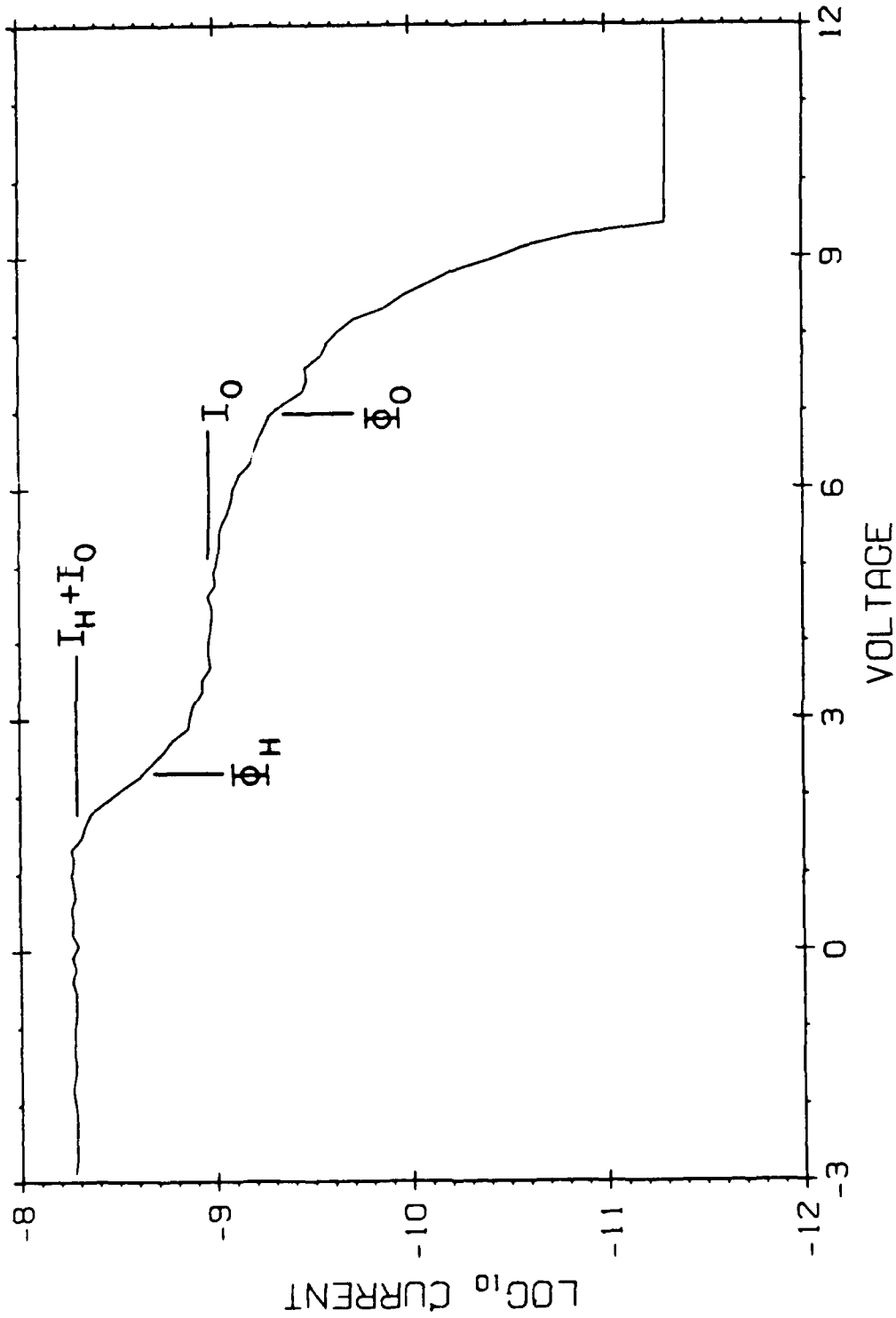


Figure 6-4 Example of current-voltage curve obtained from one "sweep" of the voltage on a Retarding Potential Analyzer (RPA). The ion temperature, drift velocity, densities, and aperture potential can be determined from this I-V curve.

7. PUBLICATIONS

The following papers and publications were done in whole or part on contract F19628-86-K-0045:

- (1) Basinska, E.M., W.J. Burke, Su. Basu, F.J. Rich and P.F. Fougere. "Low-Frequency Modulation of Plasmas and Soft Electron Precipitation Near the Dayside Cusp", *J. Geophys. Res.*, 92, 3304-3314, 1987.
- (2) Rich, F. J., M. S. Gussenhoven, and M. E. Greenspan. "Using simultaneous particle and field observations on a low altitude satellite to estimate Joule heat energy flow into the high latitude ionosphere", *Annales Geophysicae*, 5A, 527-534, 1987
- (3) Basinska, E.M. and W.J. Burke, "Ionospheric Signatures of the FTE in the S3-2 Data", *Eos, Trans. AGU*, 69, 450, 1988.
- (4) Weimer, D. R., N. C. Maynard, W. J. Burke, and M. Sugiura, "Stationary auroral current oscillations resulting from the magnetospheric generator", *J. Geophys. Res.*, 93, 11436, 1988.
- (5) Weimer, D. R., "Auroral E-fields from DE-1 and -2 at magnetically conjugate points", *Adv. Space Res.*, 8, (9)373, 1988.
- (6) Basinska, E.M., W.J. Burke and M.A. Heinemann, "A Users's Guide to Locating Flux Transfer Events in Low-Altitude Satellite Measurements: An S3-2 Case Study", *J. Geophys. Res.*, 94, 6681-6691, 1989.
- (7) Basinska, E.M., W.J. Burke, N.C. Maynard, J.D. Winningham, L.H. Brace and J.A. Slavin, "Intense Electric Fields at the Equatorward Boundary of the Dayside Cusp", *Eos, Trans. AGU*, 70, 1296, 1989.

- (8) Greenspan, M. E., "Origins of enhanced field-aligned current at the edge of an auroral arc", *J. Geophys. Res.* 94, 12,037-12,042, 1989.
- (9) Maynard, N.C., T.L. Aggson, E.M. Basinska, W.J. Burke, P. Craven, W.K. Peterson, M. Sugiura and D.R. Weimer, "Magnetospheric Boundary Dynamics: DE-1 and DE-2 Observations near the Magnetopause and Cusp", (to be) submitted to *J. Geophys. Res.*, 1990.
- (10) Baker, K. B., R. A. Greenwald, J. M. Ruohoniemi, J. R. Dudeney, M. Pinnock, P. T. Newell, and M. E. Greenspan, "Simultaneous HF-radar and DMSP observations of the cusp", submitted to *Geophys. Res. Lett.*, 1990.
- (11) Newell, P. T., E. R. Sanchez, C.-I. Meng, W. J. Burke, and M. E. Greenspan, "Identification and observation of the plasma mantle at low altitude", to be submitted to *J. Geophys. Res.*, 1990.
- (12) Weimer, D. R., N. C. Maynard, W. J. Burke, C. Liebrecht, "Polar cap potentials and the auroral electrojet indices", submitted to *Planetary and Space Science*, 1990.